Methane in Zackenberg Valley, NE Greenland: Multidecadal growing season fluxes of a high Arctic tundra

Johan H. Scheller[1,2], Mikhail Mastepanov[1,3], Hanne H. Christiansen[2], Torben R. Christensen[1]

[1]Department of Bioscience, Arctic Research Centre Aarhus University, Roskilde, Denmark

[2]Arctic Geology Department, The University Centre in Svalbard, Longyearbyen, Norway

[3]Oulanka research station, University of Oulu, Finland

Correspondence to: Johan H. Scheller (jscheller@bios.au.dk)

Abstract. The carbon balance of high-latitude terrestrial ecosystems plays an essential role in the atmospheric concentration of trace gases, including carbon dioxide (CO_2) and methane (CH_4). Increasing ~~levels of~~ atmospheric methane levels have contributed to ~20 % of the observed global warming since the pre-industrial era. Rising temperatures in the Arctic are expected to promote the release of methane from Arctic ecosystems. Still, existing methane flux ~~data collection~~measurement efforts are sparse and highly scattered, and further attempts to assess the landscape fluxes over multiple years are needed.

Here we ~~use multiyear~~ combine multi-year July–August methane flux monitoring (2006–2019) from automated flux chambers ~~located on the fringe of a fen area~~ in the ~~center~~central fens of Zackenberg Valley, northeast Greenland, ~~from July and August (2006–2019). Direct measurements of methane~~ with several flux measurement campaigns on the most common vegetation types in the valley to estimate the landscape fluxes ~~showed high variability, with mean July–August fluxes ranging from 0.26 to 3.41 mg CH_4 m^{-2} h^{-1}~~over 14 years. Methane fluxes based on manual chamber measurements are available from campaigns in 1997, 1999–2000, and in shorter periods from 2007–2013 and ~~have been~~were summarized in several published studies. ~~Fluxes from the multiyear monitoring were combined with~~The landscape fluxes ~~from the most common vegetation types, measured in 2007,~~are calculated for the entire valley floor and a ~~detailed vegetation cover map to assess~~smaller subsection of the valley floor, containing the ~~methane flux on a landscape scale and its variability over time.~~ productive fen area, Rylekærene.

When integrated for the valley floor, the estimated July–August landscape fluxes~~, estimated in the current study for the 2006–2019 period,~~ were low compared to the single previous ~~estimations. For the full study area covering~~estimate, while the ~~valley floor, the~~ landscape fluxes for Rylekærene were comparable to previous estimates. The valley floor was a net methane source during ~~these months was~~ July–August, with estimated ~~as~~mean methane fluxes ranging from 0.~~06~~18 to 0.~~83~~67 mg ~~CH_4~~ m^{-2} h^{-1} ~~and as~~. The mean methane fluxes in the fen-rich Rylekærene were substantially higher, with fluxes ranging from 0.~~26~~98 to 3.~~45~~26 mg ~~CH_4~~ m^{-2} h^{-1} ~~for the central fen-rich areas.~~ .

A 2017–2018 erosion event indicates that some fen and grassland areas ~~along the river~~ in the center of the valley are becoming unstable following pronounced fluvial erosion and a prolonged period of permafrost warming. Although such physical disturbance in the landscape can disrupt the current ecosystem–atmosphere flux patterns, even pronounced future erosion ~~along the river~~of ice-rich areas is unlikely to impact methane fluxes ~~at~~on a landscape ~~-~~scale significantly. Instead, projected changes in future climate in the valley play a more critical role.

The results show that ~~multiyear~~multi-year landscape methane fluxes are highly variable ~~at~~on a landscape ~~-~~scale and stress the need for long-term spatially distributed measurements in the Arctic.

1 Introduction

~~For decades, tundra ecosystems have been subject to attention concerning changing~~It was early in climate~~. The~~ change research recognized that the Arctic is ~~known to be~~ particularly prone to increasing temperatures, and considerable changes to ecosystems at high latitudes were to be expected ~~(IPCC, 1990). Further, high latitude wetlands have, for a long time, been recognized as a significant contributor to the global atmospheric budget of methane (CH_4). In the first global budget, the wetland source was estimated at 130 to 260 Tg y^{-1} of a total atmospheric burden of 529 to 825 Tg y^{-1} (Ehhalt, 1974).~~(IPCC, 1990). For decades, hence, tundra ecosystems have been subject to attention concerning changing climate. Further, high latitude wetlands have, for a long time, been recognized as a contributor to the global atmospheric budget of methane (CH_4). In the first global budget, the tundra source was an estimated 1.3 to 13 Tg y^{-1} of a total atmospheric burden of 529 to 825 Tg y^{-1} (Ehhalt, 1974). This term and the overall atmospheric budget have changed remarkably little during nearly 50 years of research, with ~~a more recent estimate ranging from 140 to 280 Tg y^{-1} (Christensen, 2014). It still forms the background for the concern that with Arctic ecosystems warming, including the wetland source regions, increasing emissions can start a positive feedback in the climate system.~~emission estimates for all global wetlands ranging from 140 to 280 Tg y^{-1} in the 1970s as well as in the 2010s (Christensen, 2014). This still also forms the background for the concern that with Arctic ecosystems warming, the so far modest wet tundra emissions may increase and start a positive feedback in the climate system (Knoblauch et al., 2018). In addition to Arctic warming, landscape changes such as permafrost thaw affecting tundra ecosystems and lake formations have been identified as possible hotspots for increased emissions ~~(Schuur et al., 2015; Walter Anthony et al., 2018).~~(Schuur et al., 2015; Walter Anthony et al., 2018). Also, coastal and further offshore marine sources are subject to possible changed emissions in the Arctic ~~(Shakhova et al., 2014; Thornton et al., 2020)~~(Shakhova et al., 2014; Thornton et al., 2020), but these are not dealt with here. Overall, these concerns led to early and still continuing efforts at quantifying more closely the Arctic natural emissions and their sensitivity and dynamics in relation to climate change.

Studies of tundra methane emissions in several parts of the Arctic were initiated between the 1970s and 1990s ~~(Svensson and Rosswall, 1984; Whalen and Reeburgh, 1988; Morrissey and Livingston, 1992; Christensen, 1993). The~~(Svensson and Rosswall, 1984; Whalen and Reeburgh, 1988; Morrissey and Livingston, 1992; Christensen, 1993). Zackenberg Valley in northeast Greenland was one of the first high Arctic sites to be added to the circumpolar map of methane flux studies in 1997 ~~(Christensen et al., 2000) after the start of the Zackenberg Ecological Research Operations (ZERO) in 1995 (Meltofte et al., 2008).~~(Christensen et al., 2000) after the start of the Zackenberg Ecological Research Operations (ZERO) in 1995 (Meltofte et al., 2008). Since then, the valley has seen several different methane flux studies, and methane monitoring became part of the Greenland Ecosystem Monitoring (GEM) program in 2007 ~~(Mastepanov et al., 2013). ~~(Mastepanov et al., 2013). With numerous short-

term research projects, the monitoring has led to the availability of a unique, large number of years with observations of fluxes compared to any other location in the Arctic.

The overarching background for the sizeable emissions in the Arctic is that waterlogged undisturbed soil environments host stable anaerobic environments with optimal conditions for methanogenic activity. Compared with tropical wetlands influenced heavily by the seasonality of flooding (Nisbet et al., 2019), the arctic source areas tend to be more stable geographically. Their emissions subject to the balance between the production at depth and the microbial oxidation in the aerobic surface layer. However, through recent decades, many factors such as nutrients, plant species composition, topography/hydrology have been found to influence will modulate the size of the emissions (AMAP, 2015). From a landscape perspective, the constantly emitting wet soil environments are surrounded by and intermixed with uplands, glaciers, lakes, and rivers, all with their distinct and, in some cases, very different methane flux characteristics. It is rare that a comprehensive analysis of both these small-scale controls and spatial heterogeneity is possible simply due to a lack of locations where enough studies of different kinds have been conducted. Zackenberg Valley is here unique, with such a wide range of studies available.

Here we compile all methane flux studies conducted so far in ~~the~~Zackenberg valley with the objectives to 1) review the combined information from these studies on temporal and spatial variability of methane fluxes in a composite high Arctic landscape and 2) assess the sensitivity of the measured fluxes as they respond to climate warming or local changes. ~~The~~A large number of studies and multiple years of observations, along with the addition of flux measurements from a recent gully, provide a unique opportunity to disentangle the effect of different processes and quantify their relative influence on the fluxes ~~at the~~on a landscape ~~-~~scale. These processes can broadly be grouped as 1) climate variability and the projections for a gradual warming, 2) increased erosion of vegetated surfaces.

The challenge is to quantify the sensitivity of the landscape fluxes to these factors individually to allow for ~~a~~ quantitative analysis of how the factors combine and compare in terms of sensitivity to established climate warming scenarios. To conduct this study, we use a combination of published data and new measurements of methane fluxes from a recently eroded gully near the Zackenberg Research Station and its immediate surroundings.

2 Materials and methods

2.1 Site description

~~Zackenberg Valley is located at 74.47° N, 20.55° W, between 0 to 200 m above sea level (m.a.s.l.) in northeast Greenland. The climate of Zackenberg Valley is high Arctic (Meltofte and Rasch, 2008), with an annual mean air temperature of −9.0 °C, which increased by 0.06 °C year^{-1} in the 1996–2014 period (Abermann et al., 2017). The warmest month is July, with a mean temperature of 6.3 °C (1997–2014) (Pedersen et al., 2016), and freezing~~

~~temperatures rarely occurring during the 4–6 weeks of high summer (Hansen et al., 2008). Annual precipitation is measured from 1 September to 31 August and ranged from 222 to 547 mm water equivalent, with a mean of 367 mm (1996–2014). The timing of 80 % snowmelt at the valley floor varies from 30 May (DOY 150) to 6 July (DOY 187) between 1999 and 2014 (Pedersen et al., 2016). Continuous permafrost underlies the valley (Christiansen et al., 2008), and the active layer (AL) reaches a maximum depth of 0.58 to 0.85 m, increasing at a rate of 0.74 cm year^{-1} (1996–2019) at the ZEROCALM-1 site (Christensen et al., 2020a) near the climate station at the valley floor. Figure 1a shows the development of July–August soil and air temperatures since 1997 at 0.2 m depth and 2 m height measured at the climate station. The timing of snowmelt in the study area (Fig. 1b) varies significantly between years. During July and August, there is so far no clear trend toward drier or wetter conditions for both the heath areas (Fig. 1c) and the fens~~

2.1.1 Study area

Zackenberg Valley is located at ~~the automated flux chambers (AC) site (Fig. 1d) from the mid-2000s and forward.~~

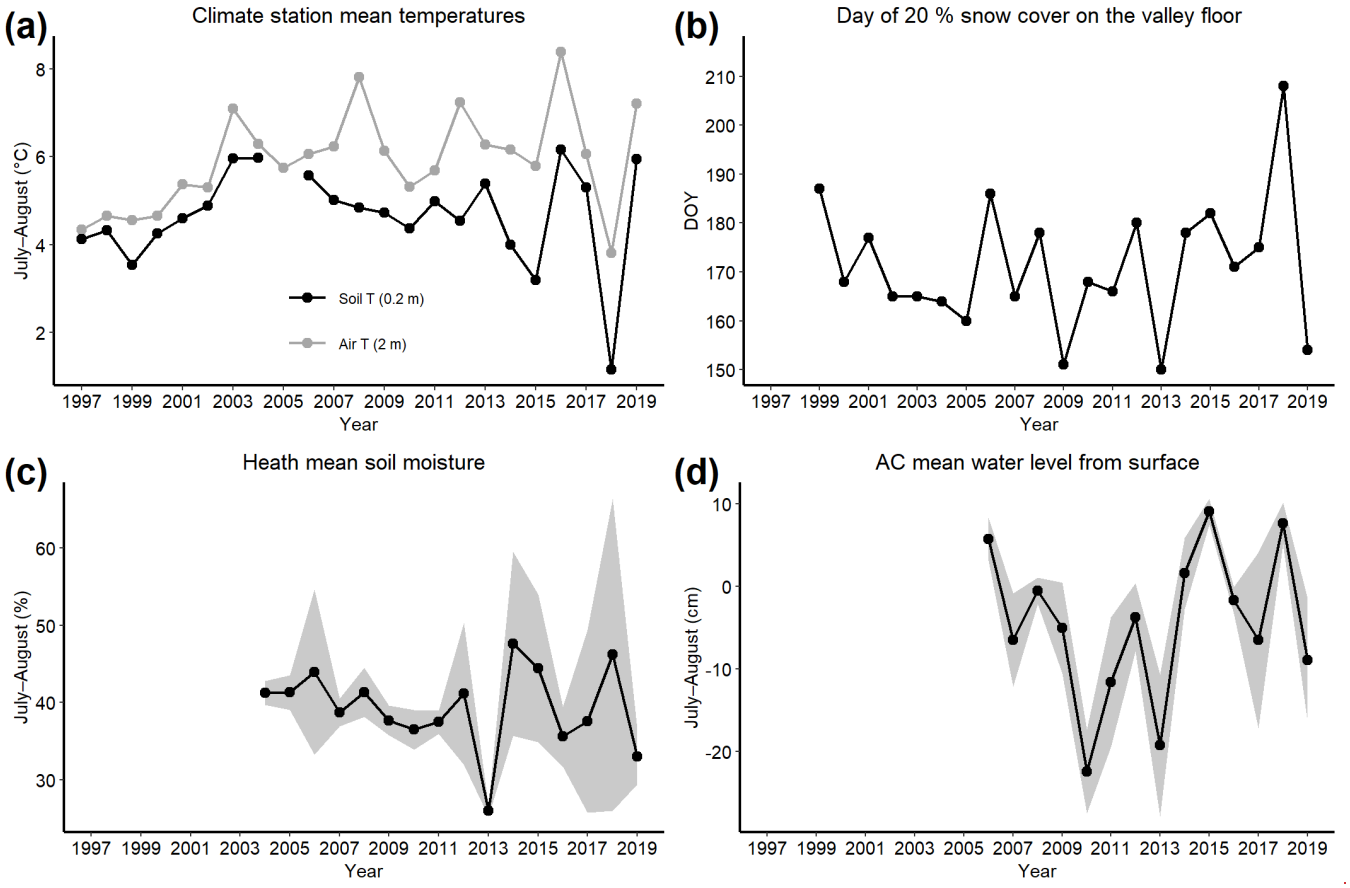

~~**Figure 1: (a) July–August mean temperatures measured at the Zackenberg climate station. (b) Timing of**~~74.47° N, 20~~**% remaining snow cover on the valley floor with 1999–2014 data from Pedersen et al. (2016). (c) July–August mean soil moisture at the Mix-1 heath site in the lower valley with standard deviation (SD) as shading. (d) July–August mean water level relative to the surface measured close to chamber 1 at the AC site with SD as shading. Please note the differences in the time axes. *Data sources: GEM ClimateBasis and GeoBasis Zackenberg*.~~

.55° W in northeast Greenland. The study area ~~in the valley~~ follows the boundaries used in ~~Søgaard et al. (2000). The area~~Søgaard et al. (2000) and covers the core monitoring and research projects area of the GEM program (Zone 1A) below 200 m~~.a.s.l., covering~~ above sea level, encompassing a total area of ~16 km^2 on the valley floor (Fig. ~~2~~1). The vegetated areas consist of continuous and hummocky fens, grasslands, *Salix* snowbeds, and *Cassiope* and *Dryas* heaths. Common species in the fens include *Dupontia psilosantha* and *Eriophorum scheuchzeri*, and graminoids, including *Arctagrostis latifolia*, *Eriophorum triste*, and *Alepecurus alpinus* covers the grassland areas. ~~(Bay, 1998)~~ (Bay, 1998).

~~A subdivision of the valley study area is~~ Rylekærene~~,~~ partly covers the valley floor study area and consists of a 1.3 km^2 patterned wet tundra ecosystem dominated by fen areas and divided by drier patches of heaths and grasslands in the central part of the valley ~~(Tagesson et al., 2013).~~(Tagesson et al., 2013). Rylekærene has been a subject of several methane flux studies since the mid-1990s, and several sites within the area have been in use (Fig. ~~2).~~ 1).

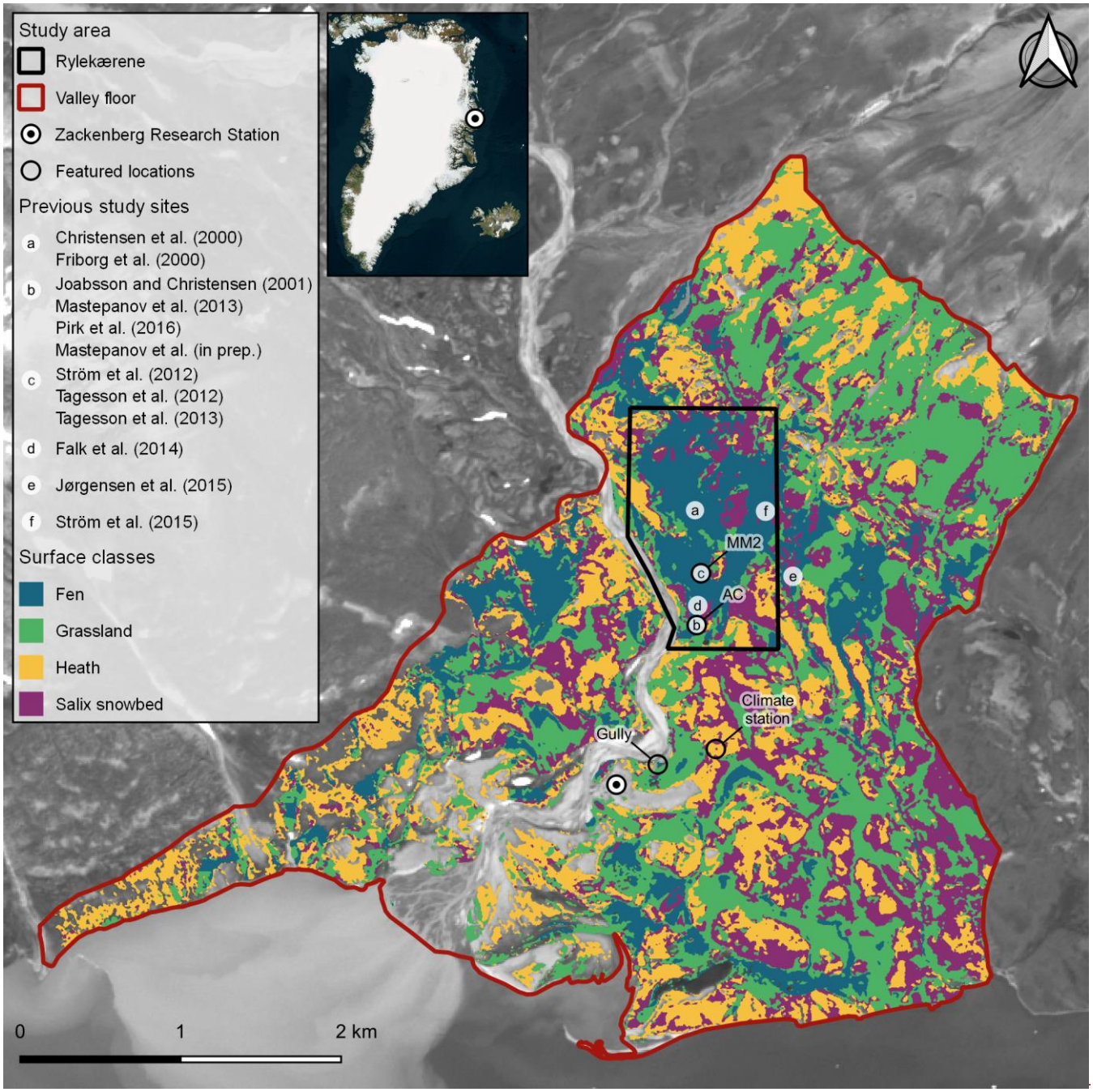

~~**Figure 2: The study area with dark red and black boundaries showing**~~A backward erosion gully, previously referred to as 'thermokarst' (Christensen et al., 2020b), extends from Gadekæret, a small fen area close to Zackenberg Research Station in the ~~**valley floor study area and Rylekærene in Zackenberg (74.47° N, 20.55° W) and the approximate location of previous study sites marked with letters. The two gas monitoring sites, AC and MM2, are found at the same places as study sites b and c, marked with black circles. Colored areas show the spatial distribution of the four main surface classes used in this study. Areas not covered by the four classes take up 16.9 % of the valley floor and 3.6 % of Rylekærene.** ***Data sources: HyMap hyperspectral imaging campaign (7 August 2000), ESA Copernicus Sentinel-2 (Grayscale, 16 July 2019), and © Microsoft 2021.***~~

~~The first methane flux measurements in Rylekærene were carried out in 1997 in studies by Christensen et al. (2000) and Friborg et al. (2000) using manual flux chamber measurements and the eddy covariance (EC) method in the center of the fen area (Fig. 2a). In the south end of Rylekærene, less than 600 m south of the EC site, Joabsson and Christensen (2001) measured methane fluxes in 1999–2000 (Fig. 2b). Close to this site, the AC setup has measured~~

methane and CO_2 fluxes along a topographic gradient from a wet fen area and a drier grassland area starting in 2005. The AC site is a central part of the GeoBasis subprogram of GEM (Mastepanov et al., 2008; Mastepanov et al., 2013).

Tagesson et al. (2012)valley (Fig. 1). The measured methane and CO_2 fluxes by gradient EC methods at a site in the center of Rylekærene in 2008 and 2009. This site (Fig. 2c) is located ~250 m north of the AC site and was later promoted to a permanent EC CO_2 flux installation for measurements in the GeoBasis subprogram under the MM2 (MicroMet 2) name (Lund et al., 2008–2011; Stiegler et al., 2016).

In 2007, methane fluxes of the most common vegetation types were measured at 55 plots in a ~600 m^2 area in the center of Rylekærene, about 300 m north of the AC site (Tagesson et al., 2013), and 50 to 150 m east of the current location of MM2.

More recently, several studies focused on areas outside the permanent AC and MM2 sites, including Falk et al. (2014) (Fig. 2d) and Jørgensen et al. (2015) (Fig. 2e) towards the eastern border of Rylekærene, and Ström et al. (2015) in between the AC site and MM2 (Fig. 2f).

A large dendritically shaped gully formed rapidly during July 2018, most likely triggered by substantial lateral erosion of up to 4.7 m in an outer bend of the river after a glacier lake outburst flood (GLOF) in August 2017 (Tomczyk et al., 2020),(Tomczyk et al., 2020), right where the gully ends. This gully, previously referred to as 'thermokarst', extends from Gadekæret, a small fen area close to Zackenberg Research Station (Christensen et al., 2020b). The gully is up to 1 to 4 m deep, up to 8 m wide, and ~50 m long in the longest flow direction. This process is different from thermokarst and is similar to the active development of a gully in the northern part of Zackenberg Valley in 1999 (Christiansen et al., 2008).(Christiansen et al., 2008). The retrogressive, branching pattern of the gully most likely occurs along with ice -wedges in the area. Meltwater from a large snowpack located in Gadekæret in early 2018 has most likely saturated the thawed sediments and thermally eroded the ice -wedges, causing sediment transport from the site and into the river.

The gully was monitored closely during the 2019 field season, but its development had come to a halt.ceased. Standing water covered the bottom of the gully during August 2018, and elevated methane concentrations were detected in the area (Christensen et al., 2020b).(Christensen et al., 2020b). In 2019, the bottom of the gully had dried out, and methane concentrations were no longer elevated.

2.2 Measurements

2.2.1 Fluxes from mobile and automated chambers

Most of the previous studies in the research area were based on mobile flux chambers and stationary automatic chambers, which utilized measured changes in methane concentration over time inside a chamber to estimate surface fluxes. The chamber was sealed off to all sides but the bottom during each measurement, isolating the flux estimates to a specific time and area, analogous to the approach described by, e.g., Crill et al. (1988) and Livingston and Hutchinson (1995). Methods vary between the studies, with differences in gas analyzers, chamber designs,

measurement time, replication numbers, sampling frequency, and the length of the study periods. The similarities and differences are summarized in Table 1.

Table 1: Flux chamber measurements in Zackenberg Valley vary in several ways between studies. Please see each study for a detailed description of the methods. Only the data used in this study are included in the table, i.e., unmanipulated and control plots.

Publication and study year	Gas analysis	Chamber design	Sampling time	Plots	Measurement frequency

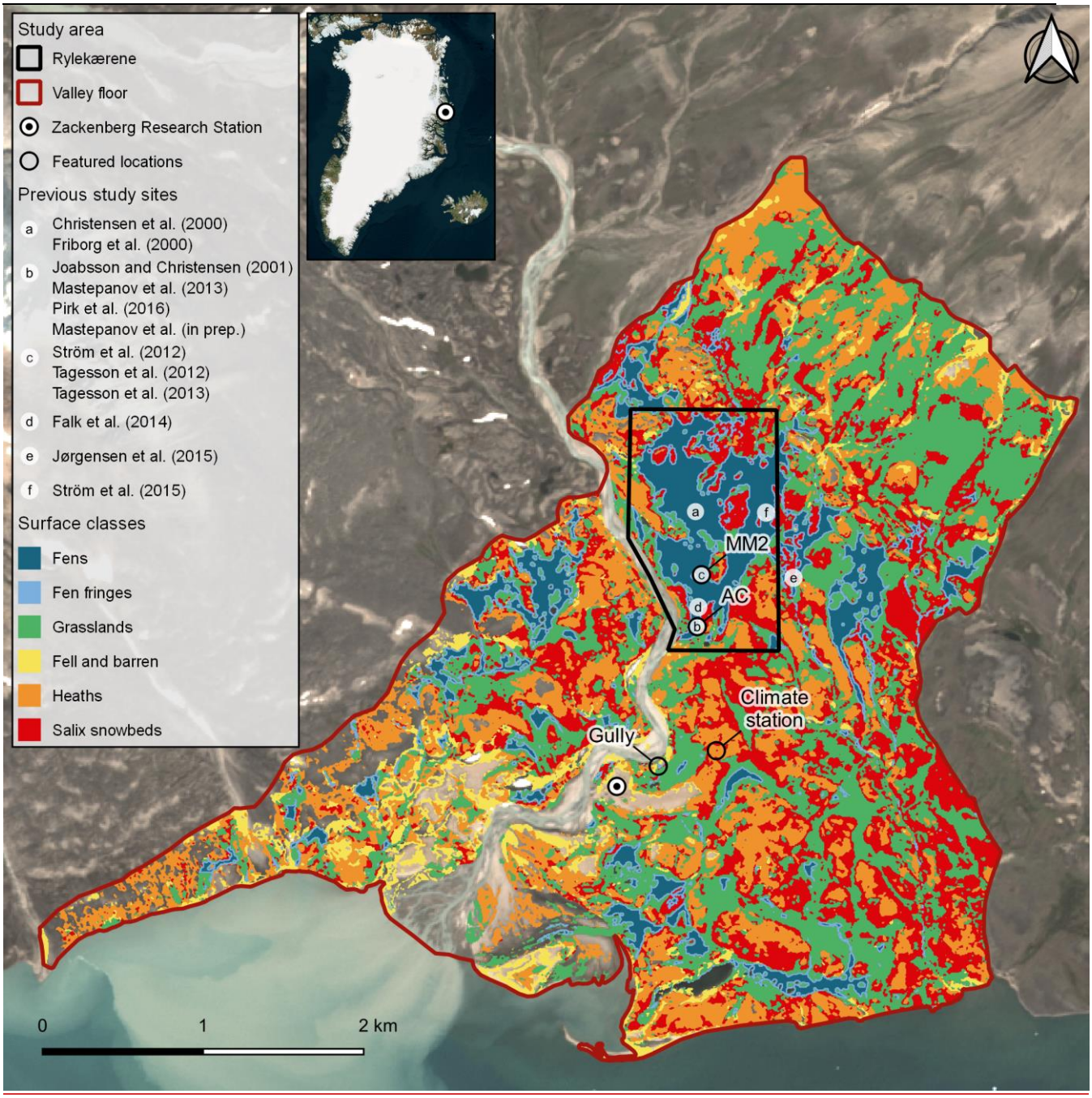

Figure 1. The study area with dark red and black boundaries showing the valley floor study area and Rylekærene in Zackenberg (74.47° N, 20.55° W) and approximate locations of previous study sites are marked with letters. The two gas flux monitoring sites, AC and MM2, are found at the same places as study sites b and c, marked with black circles. Colored areas show the spatial distribution of the six surface classes used in this study. ***Data sources: HyMap hyperspectral imaging campaign (7 August 2000) (Elberling et al., 2008), ESA Copernicus Sentinel-2 (16 July 2019), and © BING Maps 2021.***

Table 1 shows the coverage of each surface class compared to the valley floor and Rylekærene areas in both absolute and relative terms, based on hyperspectral aerial data from (Elberling et al., 2008), which improved on a manual land cover classification by Bay (1998). Zackenberg River has changed its course since 2000 after multiple GLOF events (Søndergaard et al., 2015; Tomczyk and Ewertowski, 2020), and we adjusted the land cover classification map to fit the extent of the river in a 2014 orthomosaic of the entire study area (COWI, 2015).

Table 1. Absolute and relative area distributions for the six main surface cover classes in the two study areas shown in Fig. 1, updated to the Zackenberg River extent in 2014. The 'fen fringe' surface class covers the outer 10 m of the fen areas.

Surface class	Valley floor in m^2 (% of the area)	Rylekærene in m^2 (% of the area)
Fens	983,920 (6.2 %)	464,816 (36.6 %)
Fen fringes	920,504 (5.8 %)	176,502 (13.9 %)
Grassland	4,429,921 (27.9 %)	176,135 (13.9 %)
Fell and barren	964,643 (6.1 %)	7,854 (0.1 %)
Heaths	3,434,361 (21.6 %)	138,692 (10.9 %)
Salix snowbeds	3,244,606 (20.4 %)	265,979 (20.9 %)
Other	2,891,691 (18.1 %)	41,325 (3.7 %)
Total	15,905,003 (100 %)	1,271,303 (100 %)

2.1.2 Climatology

The study area is as high Arctic (Meltofte and Rasch, 2008), with mean annual air temperature and precipitation of −8.6 °C and 253 mm (2008–2018) (López-Blanco et al., 2020). Continuous permafrost underlies the valley (Christiansen et al., 2008), and the active layer (AL) reaches a maximum depth of 0.58 to 0.85 m, increasing at a rate of 0.74 cm $year^{-1}$ (1996–2019) at the ZEROCALM-1 site (Christensen et al., 2020a) near the climate station at the valley floor.

2.2 Methane flux measurements

2.2.1 Measurements in Rylekærene

The first methane flux measurements in Rylekærene were carried out in 1997 in Christensen et al. (2000) and Friborg et al. (2000). They used manual flux chamber measurements and the eddy covariance (EC) method in the center of the fen area (Fig. 1, site a). In the south end of Rylekærene, Joabsson and Christensen (2001) measured methane fluxes in 1999–2000 (Fig. 1, site b). An automated chamber setup was added nearby in 2005. The automated chambers (AC) measure methane and CO_2 fluxes along a topographic gradient from a wet fen to a heath area. The AC site is a part of the GeoBasis subprogram of GEM (Mastepanov et al., 2008; Mastepanov et al., 2013). Tagesson et al. (2012) measured methane and CO_2 fluxes by gradient EC methods at a site in the center of Rylekærene in 2008 and 2009. This site (Fig. 1, site c) is located ~250 m north of the AC site and was later promoted to a permanent EC CO_2 flux installation for measurements in the GeoBasis subprogram under the MM2 (MicroMet 2) name (Lund et al., 2008–2011; Stiegler et al., 2016).

In 2007, Tagesson et al. (2013) measured methane fluxes of the most common vegetation types in a ~600 m^2 area in the center of Rylekærene, 50 to 150 m east of the current location of MM2.

More recently, several studies focused on areas outside the permanent AC and MM2 sites, including Falk et al. (2014) (Fig. 1, site d), and Jørgensen et al. (2015) (Fig. 1, site e) toward the eastern border of Rylekærene. Ström et al. (2015) measured fluxes in between the AC site and MM2 (Fig. 1, site f). The length of these campaigns, their onset compared to the beginning of the growing season, the sampling area, and strategy vary between studies. Figure 2 shows a timeline of methane flux campaigns from published studies and data from the GEM database.

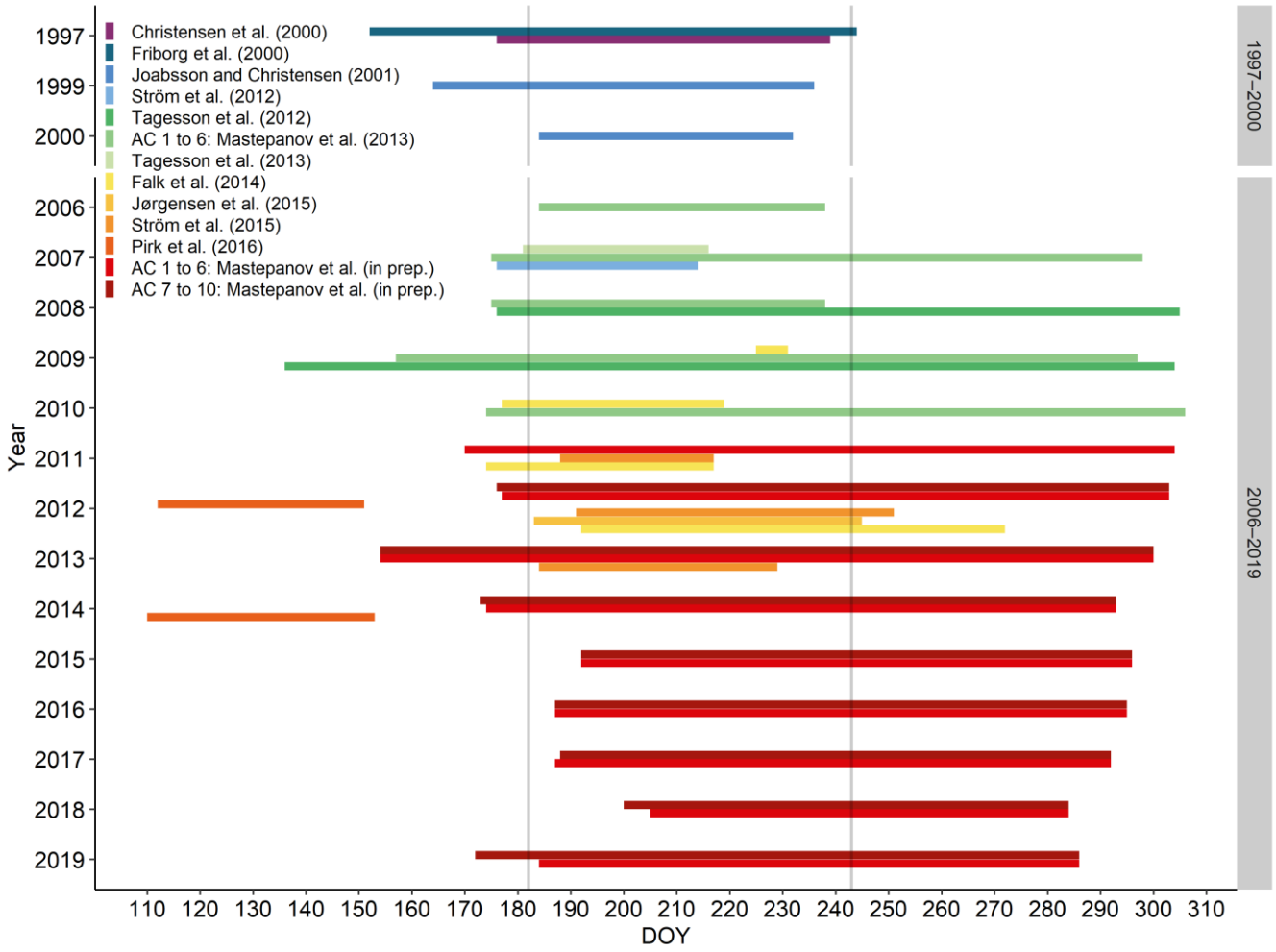

Figure 2. Timeline of methane measurement campaigns and monitoring in individual years, shown as the day of year (DOY). Colors show different publications, and the two vertical grey bars show 1 July and 31 August in non-leap years. Please note that the years 2001–2005 are left out, as no published studies focusing on methane fluxes in undisturbed areas were made in this period.

Most of the previous studies in the research area were based on mobile flux chambers, and stationary automatic chambers, which utilized changes in methane concentration measured over time inside a closed chamber to estimate surface fluxes. The chamber was sealed off to all sides but the bottom during each measurement, isolating the flux estimates to a specific time and area, analogous to the approach described by, e.g., Crill et al. (1988) and Livingston and Hutchinson (1995). Methods vary between the studies, with differences in gas analyzers, chamber designs, measurement time, replication numbers, sampling frequency, and the length of the study periods. Details on the methods are summarized in Table 2.

Table 2. Flux chamber measurements in Zackenberg Valley vary in several ways between studies. Please see each study for a detailed description of the methods. Only the data used in this study are included in the table, i.e., unmanipulated and control plots.

Publication and study year	Gas analysis	Chamber design	Sampling time	Plots	Measurement frequency
~~Christensen et al. (2000) in 1997~~	~~Duplicate syringe sample in two 10 to 15 min intervals. Analysis with a Shimadzu GC14-B gas chromatograph~~	~~13 to 30 L, aluminum dark chambers on bases permanently inserted to 10 to 20 cm depth~~	~~20 to 30 min~~	~~30 plots in five sites~~	~~Two times per week~~
~~Joabsson and Christensen (2001) in 1999–2000~~	~~Duplicate syringe samples were taken at regular intervals. Analysis with a Shimadzu GC14-B gas chromatograph~~	~~14 to 22 L, aluminum dark chambers on permanently installed bases (15 cm depth)~~	~~NA~~	~~Six plots in one site (only control plots)~~	~~One to three times per week~~
~~Ström et al. (2012) in 2007~~	~~LGR DLT200 analyzer~~	~~2.2 L, transparent chamber on permanently installed aluminum bases (set-up[1])~~	~~3 min~~	~~15~~	~~Two to four days interval~~
~~Mastepanov et al. (2013) in 2006–2010~~	~~LGR DLT100 model 908-0007~~	~~~108 L permanently installed transparent, automatic chambers~~	~~5 min~~	~~Four (2006) Six (2007–2010)~~	~~Every hour~~
~~Tagesson et al. (2013) in 2007~~	~~LGR DLT200 analyzer~~	~~10 L, transparent chamber inserted into ~2 cm notches in the ground~~	~~3 min~~	~~55 plots in seven sites~~	~~Two to three times per week~~
~~Falk et al. (2014) in 2009–2012~~	~~LGR DLT200 analyzer and Gasmet Dx 40-30 Fourier transform infrared spectrometer~~	~~41 L, transparent and dark chambers on bases permanently installed to 15 cm depth~~	~~3 to 7 min~~	~~15 plots in one site (only unmanipulated plot)~~	~~Approximately two times per week~~
~~Jørgensen et al. (2015) in 2012~~	~~LGR DLT100 analyzer~~	~~Volume NA, Transparent and dark chambers on permanent bases inserted to ~10 cm depth~~	~~10 min~~	~~40 plots in four sites~~	~~NA, 280 samples in total during four campaigns~~
~~Ström et al. (2015) in 2011–2013~~	~~Gasmet Dx 40-30 Fourier transform infrared spectrometer~~	~~41 L, transparent and dark chambers on bases permanently installed to 15 cm depth~~	~~3 to 7 min~~	~~16 to 20~~	~~Approximately two times per week~~
~~Pirk et al. (2016b) in 2012 and 2014, Mastepanov et al. (in prep.) in 2011 to 2019~~	~~LGR Greenhouse Gas Analyzer model 908-0011~~	~~~108 L permanently installed transparent automatic chambers~~	~~5 min~~	~~10~~	~~Every 90 minutes~~
Christensen et al. (2000) in 1997	Duplicate syringe sample in two 10 to 15 min intervals. Analysis with a Shimadzu GC14-B gas chromatograph	13 to 30 L, aluminum dark chambers on bases permanently inserted to 10 to 20 cm depth	20 to 30 min	30 plots in five sites	Two times per week
Joabsson and Christensen (2001) in 1999–2000	Duplicate syringe samples were taken at regular intervals. Analysis with a Shimadzu GC14-B gas chromatograph	14 to 22 L, aluminum dark chambers on permanently installed bases (15 cm depth)	NA	Six plots in one site (only control plots)	One to three times per week
Ström et al. (2012) in 2007	LGR DLT200 analyzer	2.2 L, transparent chamber on permanently installed aluminum bases (set-up[1])	3 min	15	Two to four days interval
Mastepanov et al. (2013) in 2006–2010, Mastepanov et al. (in prep.) in 2011	LGR DLT100 model 908-0007	~108 L permanently installed transparent, automatic chambers	5 min	Four (2006) Six (2007–2011)	Every hour
Tagesson et al. (2013) in 2007	LGR DLT200 analyzer	10 L, transparent chamber inserted into ~2 cm notches in the ground	3 min	55 plots in seven sites	Two to three times per week
Falk et al. (2014) in 2009–2012	LGR DLT200 analyzer and Gasmet Dx 40-30 Fourier transform infrared spectrometer	41 L, transparent and dark chambers on bases permanently installed to 15 cm depth	3 to 7 min	15 plots in one site (only unmanipulated plot)	Approximately two times per week
Jørgensen et al. (2015) in 2012	LGR DLT100 analyzer	Volume NA, Transparent and dark chambers on permanent bases inserted to ~10 cm depth	10 min	40 plots in four sites	NA, 280 samples in total during four campaigns
Ström et al. (2015) in 2011–2013	Gasmet Dx 40-30 Fourier transform infrared spectrometer	41 L, transparent and dark chambers on bases permanently installed to 15 cm depth	3 to 7 min	16 to 20	Approximately two times per week

Pirk et al. (2016b) in 2012 and 2014, Mastepanov et al. (in prep.) in 2012 to 2019	LGR Greenhouse Gas Analyzer model 908-0011	~108 L permanently installed transparent automatic chambers	5 min	10	Every 90 minutes

~~For the aims of the current study, we analyzed existing data of July–August CH_4 fluxes from manual mobile chamber measurements from 2007, published in Tagesson et al. (2013), and GeoBasis-Zackenberg automatic chamber measurements (2006–2010 published in Mastepanov et al. (2013), and 2011–2019 in Mastepanov et al. (in prep.). Details on the methods are described in these publications. Only parts of the AC flux time series were used in this study; the July–August flux includes the peak of the growing season in the valley, and it matches the timing of most of the previous studies.~~

For the aims of the current study, we combined existing data of growing season methane from the studies shown in Fig. 2 from 2006 and forward. Only parts of the AC flux time series were used in this study; the July–August flux includes the peak of the growing season in the valley, and it matches the timing of most of the previous studies.

~~In addition to this data, we carried out~~ **2.2.2 Measurements in the gully area**

We conducted 113 measurements from 23 August 2019 to 1 September 2019 in a grid covering the recent gully ~~(see Fig. 2)~~ and extending toward a small lake in the Gadekæret fen area, close to Zackenberg Research Station~~.~~ (Fig. 4).

~~The measurements took place between 9 a.m. and 7 p.m. on 43 plots located 4 to 5 m from each other in the three main surface classes in the area: fen, grassland/barren area, and the recently eroded area. Several flux measurements at each surface class were performed every day.~~

~~A metal collar was carefully installed on the ground on each plot; a dark acrylic chamber was placed over the collar for a minimum of five minutes. The footprint of the collar was 0.07 m^2; the height from the soil surface to the top of the chamber was recorded for each measurement~~The measurements took place between 9 a.m. and 7 p.m. on 43 plots located 4 to 5 m from each other in the three main surface classes in the area: fens, grasslands, and in the gully. Several flux measurements at each surface class were performed every day.

A metal collar was carefully installed on the ground on each plot; a dark acrylic chamber was placed over the collar for a minimum of five minutes. The footprint of the collar was 0.07 m^2; the height from the soil surface to the top of the chamber was recorded for each measurement ~~(~~. The height ranged from 0.26 m to 0.48 m, depending on the surface topography~~). The chamber was equipped with a fan inside and had a 3 mm vent on the side. A gas analyzer (Ultraportable Greenhouse Gas Analyzer, Los Gatos Research, USA) was connected to the chamber with a pair of 15 m long HDPE tubes~~. The chamber was equipped with a fan inside and had a 3 mm vent on the side. A gas analyzer (Ultraportable Greenhouse Gas Analyzer, Los Gatos Research, USA) was connected to the chamber with a pair of 15 m long HDPE tubes ~~and~~. The gas analyzer was continuously measuring ~~CH_4~~methane concentration in the chamber headspace at 1 Hz frequency. ~~After each sample, the chamber was ventilated for at least two minutes until the methane concentration was down to ambient concentration.~~

After each sample, the chamber was ventilated for at least two minutes until the methane concentration was down to ambient concentration.

2.3 Data processing

~~2.2.2 Hyperspectral classification~~

~~The hyperspectral remote sensing data were collected on 8 August 2000 by an airborne HyMap campaign (Palmtag et al., 2015). The image data were processed into a 5 m × 5 m resolution land cover map of Zackenberg Valley (Elberling et al., 2008), improving on a manual land cover classification by Bay (1998). Zackenberg River has changed its course since 2000 after multiple GLOF events (Søndergaard et al., 2015; Tomczyk and Ewertowski, 2020), and we adjusted the land cover classification map to fit the extent of the river in a 2014 orthomosaic of the entire study area (COWI, 2015).~~

~~2.3 Data processing~~

2.3.1 Environmental changes

Monitoring of air (2 m above ground) and soil temperature (0.20 m below ground) were summarized from 1997–2019 data (60 min resolution) from the nearby climate station (Fig. 1), operated by the GEM ClimateBasis program. Mean temperatures are calculated for July–August data (Fig. 3a). The day of 20 % snow cover in the central valley is available from Pedersen et al. (2016) for the 1999–2014 period (Fig. 3b). Day of 20 % snow cover is estimated from GeoBasis monitoring data for 2015–2019. Soil moisture data at the heath site Mix-1, monitored under the GeoBasis program, were summarized as mean soil moisture percentage with SD for July–August (Fig. 3c). Water level data were collected manually daily at the AC site chamber 1 from 2006–2019. Automatic water level data is collected for 2010–2019, with a gap in data in 2013 at two sites, one near chamber 1 and another near chamber 6, positioned slightly higher in the terrain. The mean water levels are calculated for July–August (Fig. 3d), and SD is omitted to improve the readability of the figure. Dataset specifications are available from the links under ‘Data and code availability’.

2.3.~~1~~2 Measurements from ~~mobile and~~ automated and manual chambers

Data from several sources were included in the calculation of a timeline of landscape fluxes in Zackenberg Valley. Previously published and unpublished data were compiled to estimate fluxes and SE on the six surface types (Table 3), combining mobile flux measurements and flux measurements from AC. The measurement methods are described in detail in their respective publication, but for the AC, additional steps were added after applying the same approach as Mastepanov et al. (2013). The AC flux time series was separated into two datasets: one representing a long time series from a 10 m wide transition zone at the fen fringe (chambers 1 to 6). In this area, chambers with higher numbers are generally drier. Another time series represents the changes since 2012 in the four outer chambers, located further out into the fen (chambers 7 to 10). The flux data do not show a diurnal pattern

for July and August, so all available data were used in those two months. The flux measurements were first averaged for each chamber. Mean chamber fluxes were then further averaged into a single mean methane flux for each year for all the six inner chambers. The same was done for the four outer chambers from 2012–2019.

In 2006, only four chambers were operating, and no data were available for chambers 4 and 6. Potential differences in methane flux are corrected by multiplying the mean of the available 2006 data by a coefficient based on 2007 data. This coefficient was found by dividing the mean in chambers 1, 2, 3, and 5 by the mean of all six chambers.

~~**Data from Tagesson et al. (2013) included seven different surface classes: continuous fen (*n = 154*), hummocky fen (*n = 108*), grassland (*n = 110*), *Salix* (willow) snowbeds (*n = 51*), *Vaccinium* heath (*n = 54*), *Cassiope* heath (*n = 54*), and *Dryas* heath (*n = 54*). The fluxes on the seven land cover classes were further summarized into four general classes. The two fen classes were combined, and so were the three heath classes.~~

2.3.2.1 Fen flux

The mean July–August flux for chambers 7 to 10 were then combined with the mean growing season fluxes from the other studies listed in Table 3. In the valley-wide vegetation cover map, hummocky and continuous fen were not separated into different classes, even though mean fluxes differ substantially for these two surface types ~~(see~~in, e.g., Table 3 in ~~Tagesson et al. (2013)). A~~Tagesson et al. (2013) and Table 1 in Christensen et al. (2000). Each mean flux measured in fen areas was paired with the mean flux measured at the fen fringe. Using R (R Core Team, 2021), we applied unweighted Deming linear regression on the data (n = 18, *jackknife method*, *error ratio* = 0.44, *Pearson's r* = 0.64, p-value threshold = 0.05). The approach accounts for uncertainties in both the fen fringe data and in the fen data to estimate a time series for the fen surface types for 2006–2019. The measurements used in the regression for the fen areas are summarized in Table 3.

2.3.2.2 Fen fringe flux

The mean flux from the fen fringes was estimated from the mean July–August flux measured every year in the 2006–2019 period using all the available data from chamber 1 to 6 (Table 3). The timeline of mean fluxes at the fen fringe represents the outer 10 m of all fen surfaces in the valley, shown in Fig. 1 without further processing.

2.3.2.3 Grassland flux

The grassland fluxes are held constant over the time series, with data from Tagesson et al. (2013) as input to the calculation (Table 3), while grassland fluxes from Christensen et al. (2000) are omitted due to high spatial variability and a higher average flux.

2.3.2.4 Fell and barren fluxes

Jørgensen et al. (2015) found a significant methane uptake on unvegetated fell and barren surfaces in Zackenberg Valley in 2012. These measurements were grouped into a broader 'dry tundra' class that includes *Dryas* heath. Here, we use the mean methane flux from the 'dry tundra' class but only applying it for the fell and barren areas. The mean flux from these surfaces is held constant in our landscape flux time series.

2.3.2.5 Heaths and *Salix* fluxes

The heath class in this study includes both *Cassiope*, *Dryas* and *Vaccinium* areas, and data from Christensen et al. (2000), Tagesson et al. (2013), and Jørgensen et al. (2015) are combined to calculate an average estimate for fluxes

in these areas, which are held constant over time. Jørgensen et al. (2015) used different groups in their study, where different types of heath areas fall into 'dry' and 'moist' tundra (*Cassiope* and *Salix* heath). We calculated the weighted mean flux~~, taking the different sample sizes for the separate land cover classes into account, was calculated and used for this study.~~ for each study for the heath class, and then we calculated a mean and pooled SE. Likewise, the *Salix* snowbed class was calculated in the same way as with heath, with data from the same three studies, but with only the flux from 'moist' tundra from Jørgensen et al. (2015).

~~The fluxes at the AC site were calculated from each automatic chamber measurement, using the same approach as Mastepanov et al. (2013). The flux time series was separated into two datasets: one representing a long time series from the fen fringe (chambers 1 to 6). Another time series represents the changes since 2012 in the four outer chambers, located further out in the fen (chambers 7 to 10). The flux data do not show a diurnal pattern for July and August, so all available data for each chamber were used in those two months. Data from chambers 1 to 6 were first summarized for each chamber as temporal means, highlighting the differences in fluxes from each of the six inner chambers. July–August data were then further summarized into a single mean methane flux for each year. In 2006, only four chambers were operating, and no data were available for chambers 4 and 6. The difference is corrected by multiplying the mean of the available 2006 data by a coefficient based on 2007 data. This coefficient was found by dividing the mean in chambers 1, 2, 3, and 5 by the mean of all six chambers.~~

Table 3. Summary of data and processing used in the calculation of landscape methane fluxes for the six surface classes.

Surface class	Data source	Measurement year(s)	Processing
Fens	Ström et al. (2012) (*n* = 210)	2007	Fit mean fluxes to fen fringes time series using Deming linear regression, paired by year. SE estimates from jackknife method
	Tagesson et al. (2012)	2008–2009	
	Tagesson et al. (2013) (*n* = 162)	2007	
	Falk et al. (2014) (*n* = 35–85)	2010–2012	
	Ström et al. (2015) (*n* = 80–140)	2011–2013	
	Mastepanov et al. (in prep.) (*n* = 1,465–3,432)	2012–2019	
Fen fringes	Mastepanov et al. (2013) (*n* = 3,713–8,238)	2006–2010	July–August means for chamber 1–6, SE calculated from variability in flux measurements
	Mastepanov et al. (in prep.) (*n* = 1,888–4,837)	2010–2019	
Grasslands	Tagesson et al. (2013) (*n* = 110)	2007	Constant mean flux of grasslands, SE calculated from reported SD and *n*
Fell and barren	Jørgensen et al. (2015) (*n* ~ 140)	2012	Constant mean flux' dry tundra', SE calculated from reported SD and *n*
Heaths	Christensen et al. (2000) (*n* ~ 90)	1997	Constant mean flux of *Dryas*/*Cassiope*/*Vaccinium* heaths, and 'moist'/'dry' tundra flux, first weighted average by study, pooled SE
	Tagesson et al. (2013) (*n* = 162)	2007	
	Jørgensen et al. (2015) (*n* = 280)	2012	
***Salix* snowbeds**	Christensen et al. (2000) (*n* ~ 42)	1997	Constant mean flux of all *Salix* snowbed surfaces, and 'moist tundra' flux, pooled SE
	Tagesson et al. (2013) (*n* = 51)	2007	
	Jørgensen et al. (2015) (*n* ~ 140)	2012	

2.3.3 Combining data into ~~Multiyear methane flux measurements enabled a comparison between years, and the flux estimates from chambers 1 to 6 at the fen fringe are used for a spatial upscaling of methane fluxes using R (R Core Team, 2020). The July–August mean flux for each year in the 2006–2019 period ($Flux_{AC,year}$) was divided with the 2007 July–August mean flux ($Flux_{AC,2007}$ in Eq. 1), making it comparable to the timing of the mobile chamber measurements from Tagesson et al. (2013). This calculation gave a number less than 1 in years with comparatively low flux and more than 1 in years with relatively high flux. It is used below as a coefficient ($AC_{coefficient,year}$) for estimating the landscape fluxes in the 14-year time series.~~

$$AC_{coefficient,year} = \frac{Flux_{AC,year}}{Flux_{AC,2007}} \quad (1)$$

2.3.2 Land cover classes

The four**landscape flux time series**

The six combined surface classes represent occupy most of the study areas (Rylekærene and the valley floor, Table 1). In Eq. (2), the This static areal coverage ($Area_{class}$) of the surface classes was calculated using QGIS v. 3.10.0 (QGIS.org, 2020). The flux for 2007 ($Flux_{class,2007}$) and the area-weighted flux were 3.18.1 (QGIS.org, 2021).

The area-weighted flux was calculated for the two study areas, the valley floor, and Rylekærene ($Area_{total}$)., with total areas of 15,905,003 m^2 and 1,271,303 m^2. This approach assumes no fluxes of methane flux in the remaining parts 18.1 % and 3.7 % of the study areas, including the river, delta, riverabrasion plateaus, and primarily barren areas (Fig. 2).boulder fields in the 'other' category in Table 1. The area-weighted landscape flux ($Flux_{area\ weighted,\ 2007}$) calculation is shown in Eq. (2),is calculated for each year, with fluxes in the fens and classes include fen, grassland, *Salix* snowbeds, and heathfen fringes being the only to change over time.

$$Flux_{area\ weighted,2007} = \frac{\sum(Flux_{class,2007} \times Area_{class})}{Area_{total}} \quad (2)$$

2.3.3 Combining data into a landscape flux time series

An area-weighted landscape methane flux for each measurement year ($Flux_{year}$) is estimated by combining Eq. (1) and Eq. (2) in Eq. (3). The area-weighted mean landscape flux in 2007 ($Flux_{area\ weighted,\ 2007}$) is multiplied with the coefficient representing the relative changes in mean flux relative to 2007 ($AC_{coefficient,\ year}$), creating a time series of July–August fluxes from 2006 to 2019.

$$Flux_{year} = Flux_{area\ weighted,2007} \times AC_{coefficient,year} \quad (3)$$

2.3.4 Fluxes in the gully area

In the recently eroded gully area, the fluxes in 2019 were calculated using the ordinary least square linear (OLS) regression described in Pirk et al. (2016a). Of the 113 measurements, 102 had a significant ($p < 0.05$) regression slope. The remaining 11 measurements were found on both the grassland areas and on recently eroded surfaces. They showed an increase in concentration over time close to zero, and they are interpreted as areas with no flux. The 11 measurements are included in the calculation of the mean flux of the recently eroded surfaces in the gully. The mean flux and the standard error (SE) for all measurements were calculated by calculating the mean flux for repeated measurements for each plot. In the recently eroded gully area, the fluxes in 2019 were calculated using

~~the linear flux model (Pirk et al., 2016a). Of the 113 measurements, 102 had a significant ($p < 0.05$) regression slope. The remaining 11 measurements were found on both the grassland/barren areas and on recently eroded surfaces. They showed an increase in concentration over time close to zero, and they are interpreted as areas with a zero flux. The 11 measurements are included in the calculation of the mean flux of the recently eroded surfaces in the gully.~~

~~The mean flux and the standard error (SE) for all measurements were calculated by calculating the mean flux for repeated measurements for each plot.~~ Further averaging for their respective surface class (~~recent erosion, barren/grassland, fen~~gully, grasslands, fens) was done afterward, showing how fluxes can change in an area after an erosion event. Flux measurements from the gully area are limited to 10 days in the late growing season.

2.3.5 Valley flux and future impacts on methane emissions with increasing erosion activity

Recent active riverbank erosion in Zackenberg Valley raises the question of how the methane flux on a valley-scale will change with increasing erosion in the future, and the sensitivity to such changes is explored below. ~~The valley flux for the late 21st century is estimated based on Geng et al. (2019), Geng (personal communication, 24 April 2020), and the mean valley flux results from 2008–2015. The relative change in methane flux from present-day conditions to 2081–2100 conditions under the Representative Concentration Pathway 8.5 (RCP8.5) forced with the ECHAM5 general circulation model is estimated to increase by a factor of 2.43.~~

~~The mean July–August methane flux for the valley is here assumed to change linearly to a 2.43 times higher flux between 2016–2100, which allows us to include an intermediate time step (2041–2060). Over the same period, further erosion in the valley is simulated to assess the importance of surface erosion in Zackenberg on methane relative to changes in fluxes increasing temperatures. Multiple sites in Zackenberg Valley are subject to active erosion, and several of these sites are found along the Zackenberg River (Tomczyk et al., 2020). Here we hypothesize large-scale erosion along the river in the 21st century to improve our understanding of its importance on valley-wide methane fluxes, although an increase of eroded surface areas of this magnitude is unlikely.~~

~~The impacts on methane are estimated from a linear development in eroded surfaces from 0 m to 25 m and from 0 m to 100 m on each side of the Zackenberg River. The development change areas that act as sinks or sources of methane into eroded areas, using the mean flux measured on the recently eroded surfaces in the gully in 2019. The Zackenberg River was digitized to its extent in August 2014, when the valley was mapped in high detail (COWI, 2015). Eighty-five buffer zones were created on each side of the river, each representing one year. These buffer zones had a total width of 25 m and 100 m. The land cover types in each buffer zone were progressively eroded for the sensitivity study, and the associated change in methane flux was subtracted from the mean valley methane flux.~~

2.3.5.1 Changes in methane flux from increasing temperatures

In their study, Geng et al. (2019) compared the potential methane flux in the Zackenberg area modeled for the late 21st century with present-day conditions. They found an exponential growing season temperature–methane flux relationship based on Zackenberg and Kobbefjord data from 2008–2015. Present-day temperatures were modeled for the 1991–2010 period, and late 21st century temperatures were modeled for 2081–2100 under the Representative Concentration Pathway 8.5 (RCP8.5). Both present-day and future mean temperatures were modeled using the

ECHAM5 general circulation model to limit the cold bias in the model, and the relative increase in methane flux was +141 % (Geng, personal communication, 24 April 2020). The relative increase ranges from +114 % to +171 % when considering the lower and upper 95 % confidence bounds, see Fig. 3 in Geng et al. (2019).

We assume a linear increase in valley methane flux of +141 % for this sensitivity study, ranging from +114 % to +171 % from 2016–2100, even though this period does not fully match the modeled periods, i.e., from 1991–2010 to 2081–2100.

2.3.5.2 Sensitivity to increasing erosion activity

We establish three pathways to quantify how erosion could affect the landscape flux in Zackenberg Valley. In the first pathway, we calculate the impact on the mean valley flux if the eroded areas are growing at an annual rate equivalent to the size of the recent gully (720 m^2 y^{-1}). In the second and third pathway, the eroded area starts at 720 m^2 every year and grows to 5 and 10 times that area per year, respectively, i.e., a linear increase over 85 years from 720 m^2 y^{-1} to 3,600 m^2 y^{-1}, and from 720 m^2 y^{-1} to 7,200 m^2 y^{-1}. In this calculation, the erosion can only occur in zones with excessive ice-rich permafrost near rivers and streams. To identify these zones, we use GIS data available from Cable et al. (2018). Inside our study area (Fig. 1), we identify parts of the landscape that likely have 'excess ice-rich top 1 m permafrost' and are located near 'rivers', which include both rivers and tributaries, see Fig. 12 in Cable et al. (2018). Based on observations from the recent gully, erosion can occur up to 50 m from the rivers. Inside the identified zones, we model erosion of the size specified above and the fractional cover of surface classes. The reduction in mean flux for the eroded areas is subtracted from the landscape flux. As time goes, the eroded areas increase, causing larger impacts on the landscape flux, while all fluxes increase at the same rate as when the mean temperatures increase.

2.3.5.3 Revegetation of eroded areas

A similar gully in the northern part of the valley developed in 1999 (Christiansen et al., 2008), and it shows signs of revegetation on ~40 % of the eroded areas to grassland after 20 years. This estimate is based on a visual interpretation of 100 points randomly scattered over eroded parts within the gully in an orthophoto from August 2019. From the estimate, we set the regrowth rate equal to 2 % $year^{-1,}$ and this rate of regrowth is included in the overall calculation.

3 Results

3.1 ~~Temporal variability in flux~~Environmental changes

Figure 3a shows the development of July–August soil and air temperatures since 1997 at 0.2 m depth and 2 m height measured at the climate station. The mean July–August temperature is 5.9 °C for air temperatures and 4.7 °C for the available soil temperatures. Air temperatures increased by 0.07 °C $year^{-1}$ (1997–2019, n = 23, *Pearson's* r = 0.43, p = 0.04), while no significant linear trend is observed in the soil temperature data during the same period. The timing of snowmelt in the study area (Fig. 3b) shows substantial variations between years, from 30 (DOY 150) to 27 July (DOY 208). During July and August, there is so far no clear trend toward drier or wetter conditions for

both the heath areas (Fig. 3c) and the fens at the AC site (Fig. 3d) from the mid-2000s and forward. Measurements from chamber 6 show generally drier conditions than from chamber 1, which is located further out in the fen.

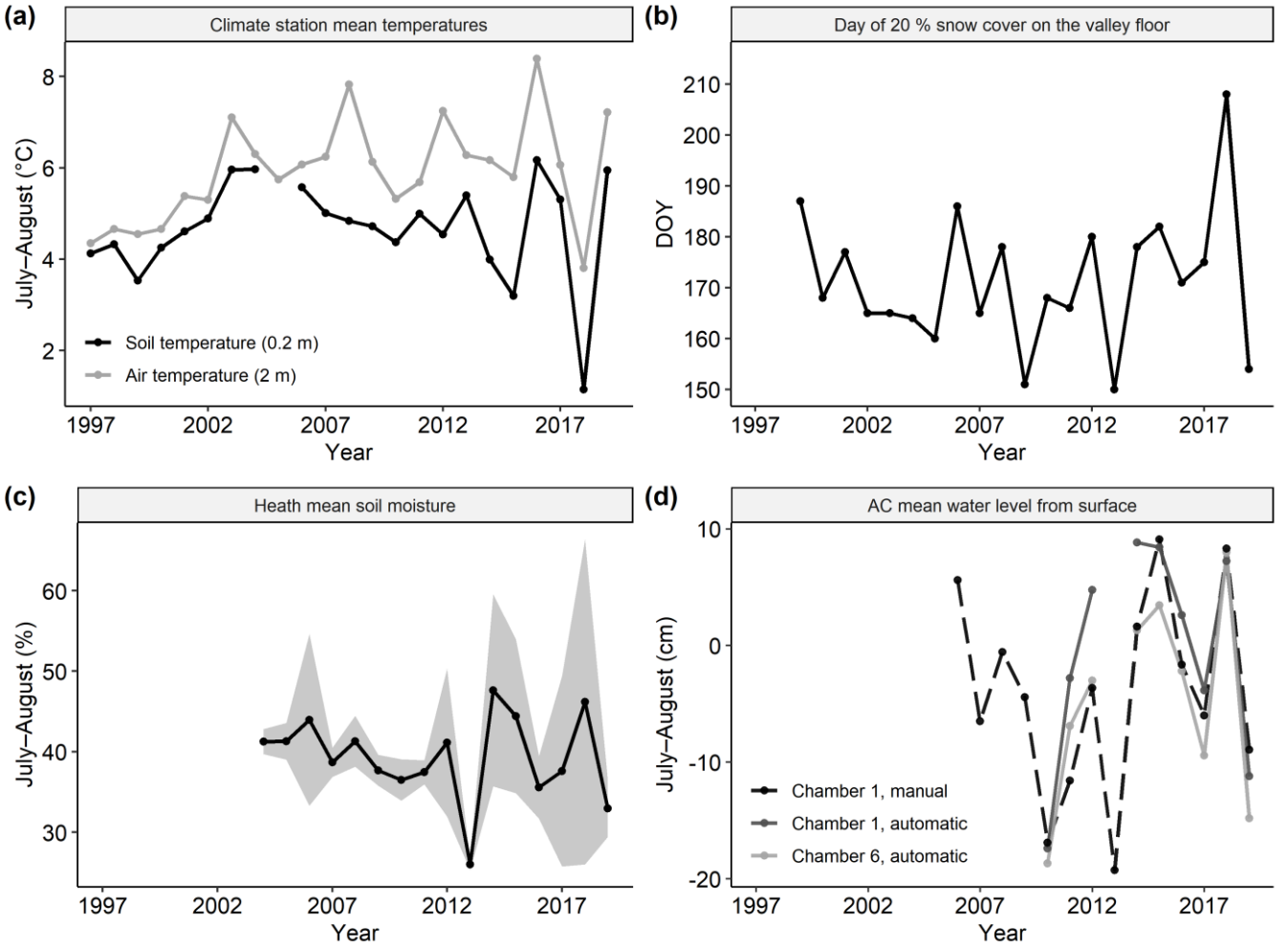

Figure 3. (a) July–August mean temperatures measured at the Zackenberg climate station. (b) Timing of 20 % remaining snow cover on the valley floor with 1999–2014 data from Pedersen et al. (2016). (c) July–August mean soil moisture at the Mix-1 heath site in the lower valley with standard deviation (SD) as shading. (d) July–August mean water level relative to the surface measured close to chamber 1.

~~From 1 July to 31 August, methane fluxes measured at six chambers available for the entire 2006–2019 period at the AC site show spatial and temporal variability both within years and between years (Fig. 3). Results for the entire growing season have earlier been published for 2006–2010, where fluctuations and patterns within years are analyzed, focusing on the variations in the mean flux of six chambers (Mastepanov et al., 2013). Treating all six chambers as replicates reveal high temporal variability for the area (red points and line in Fig. 3). The highest July–August mean flux (± SE) for all six chambers was 3.41 ± 0.57 mg m^{-2} h^{-1} in 2007. The lowest mean flux of all six chambers was 0.26 ± 0.07 mg m^{-2} h^{-1} in 2011, and the mean flux for all chambers for all 14 seasons was 1.27 ± 0.01 mg m^{-2} h^{-1}. Error bars (SE) around the mean of chambers 1 to 6 express the spatial variability between chambers for each year. The spatial variability was smallest in 2011 and the highest in 2007. Figure 3 shows no clear trend in July–August mean methane flux over the 14 years.~~

~~Not shown here are the individual mean fluxes for the four chambers operating further out in the fen since 2012. These chambers, named chambers 7 to 10, generally show higher fluxes than those measured at chamber 1 in Mastepanov et al. (2013) and Mastepanov et al. (in prep.).~~

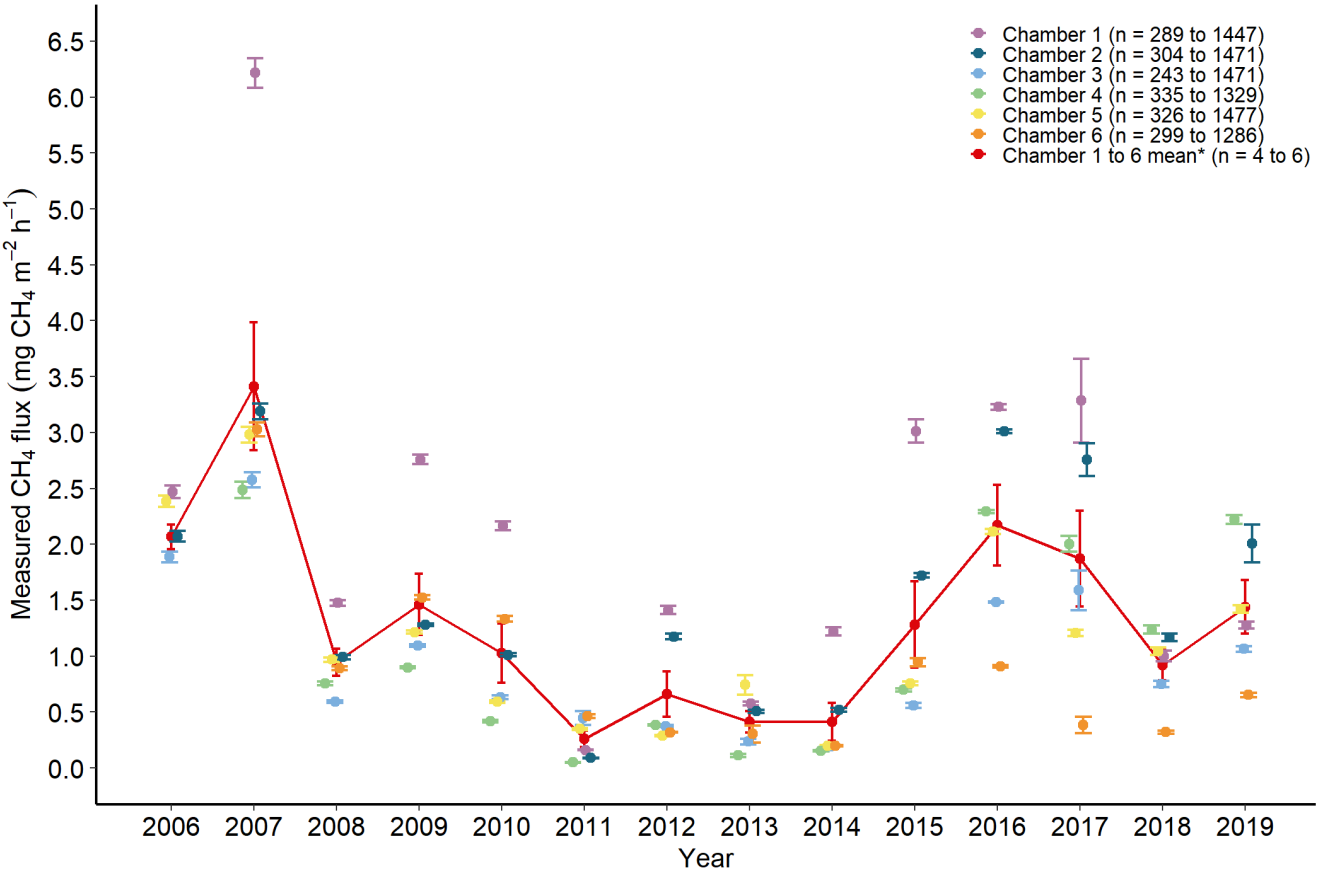

~~**Figure 3: Time series of July–August AC methane measurements from 2006–2019. Chamber 1 through chamber 6 show the temporal mean of fluxes and error bars show the SE of the temporal variability. The red dots and lines show the spatial mean of the fluxes in chambers 1 to 6 with error bars displaying the SE between chambers. The range of observations (n), as the quantity changes through time. *The SE for Chamber 1 to 6 mean is calculated from the mean of each chamber, which explains the low number of observations. *Data source: GEM GeoBasis Zackenberg*.**~~

~~3.2 Surface cover~~

~~The area of four surface classes of the valley floor and the fen-dominated Rylekærene was calculated based on HyMap data from August 2000. The surface classes used in this study are a subset of the HyMap dataset, combining heath classes and excluding 'Other' surface classes. This class includes barren areas, lakes, and rivers. The four surface classes cover most of the valley (Fig. 2), with the notable exemptions of the Zackenberg River system and the landing strip. The four surface classes cover 83.1 % of the valley study area and 96.4 % of the Rylekærene study area, where most methane studies in the valley were carried out (Fig. 2).~~

~~**Table 2** shows the coverage of each surface class compared to the valley floor and Rylekærene areas in both absolute and relative terms. The fen surface class takes up 12.1 % of the valley floor while accounting for 50.4 % of the Rylekærene study area. Grassland and heath areas are common (28.5 % and 21.8 %) in the valley floor area while being relatively less important in Rylekærene. *Salix* snowbeds take up 20.7 % and 21.1 % in the two study areas.~~

The relative composition of the two study areas is used for estimating the area-weighted methane landscape flux for the time series.

Table 2: Absolute and relative area distribution for the four main surface cover classes in the two study areas from HyMAP classification updated to the Zackenberg River extent in 2014.

Surface class	Valley floor in m^2 (% of the area)	Rylekærene in m^2 (% of the area)
Fen	1,916,658 (12.1 %)	641,368 (50.4 %)
Grassland	4,536,727 (28.5 %)	177,805 (14.0 %)
Heath	3,465,133 (21.8 %)	139,167 (10.9 %)
Salix snowbeds	3,294,996 (20.7 %)	267,819 (21.1 %)
Other (e.g. barren & water)	*2,691,489 (16.9 %)*	*45,144 (3.6 %)*
Total	15,905,003 (100 %)	1,271,303 (100 %)

3.3 Gully methane fluxes

The methane flux at the exposed, eroded surfaces of the gully was different from the flux on the nearby, undisturbed surfaces (Fig. 4). The late growing season mean methane flux of the recently eroded surfaces in the gully in 2019 was 0.05 ± 0.02 mg m^{-2} h^{-1}, with both positive and negative fluxes. The Grassland/barren surface cover in areas not disturbed by erosion shows a negative methane flux of −0.06 ± 0.01 mg m^{-2} h^{-1}. The mean methane flux in the fen was 3.83 ± 0.76 mg m^{-2} h^{-1}, more than 75 times higher than the mean flux in the gully. Methane emissions generally increased closer to the open water body of the nearby fen. The emergence of the gully marked a transition from a small methane sink to a small source for this area. The source followed an initial substantial episodic release of methane stored in exposed ice in the year when the gully appeared (Christensen et al., 2020b).

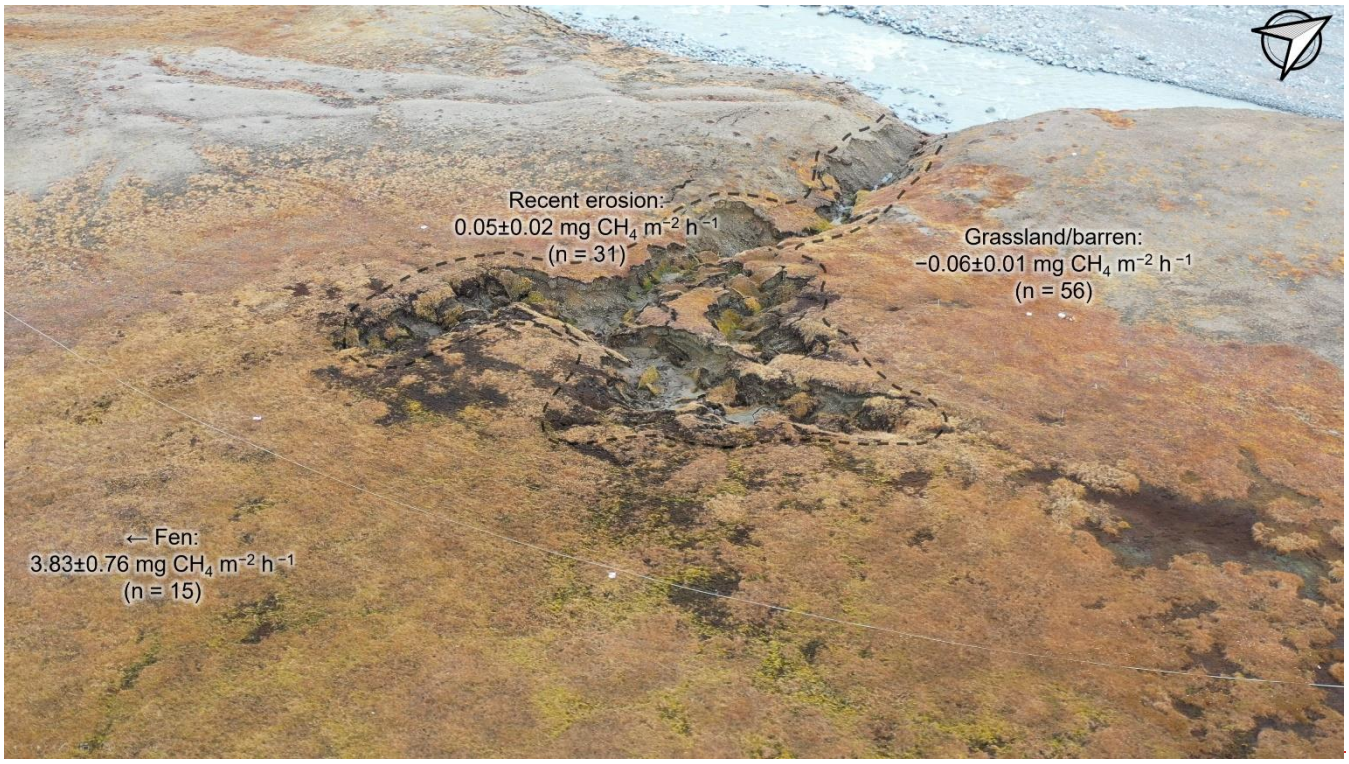

Figure 4: The gully and fen area near the Zackenberg Research Station. Numbers show the measured methane fluxes on different surface types between 23 August and 1 September 2019, when this image was captured. The dashed black line indicates the

~~approximate boundaries of the gully, which is ~50 m long and ~25 m at its widest. The nearby fen is located outside the image, ~30 m south of the gully.~~

~~3.4 Estimation of an integrated flux of methane in Zackenberg Valley~~

~~The July–August landscape flux of methane showed large interannual variability over the valley floor and Rylekærene study areas over the 14 years, 2006–2019. We observed no apparent trends (*Pearson's r* = −0.22, *p* = 0.44) over the entire period (Fig. 5). The mean flux for the 2006–2019 period was 1.32 ± 0.14 mg m^{-2} h^{-1} and 0.32 ± 0.05 mg m^{-2} h^{-1} for the Rylekærene study area and the valley floor. The methane fluxes ranged from 0.26 ± 0.03 mg m^{-2} h^{-1} in 2011 to 3.45 ± 0.31 mg m^{-2} h^{-1} in 2007 in Rylekærene and from 0.06 ± 0.03 mg m^{-2} h^{-1} to 0.83 ± 0.21 mg m^{-2} h^{-1} for the valley floor. The two study areas were net sources of methane throughout the period, although the source size changed significantly between years.~~

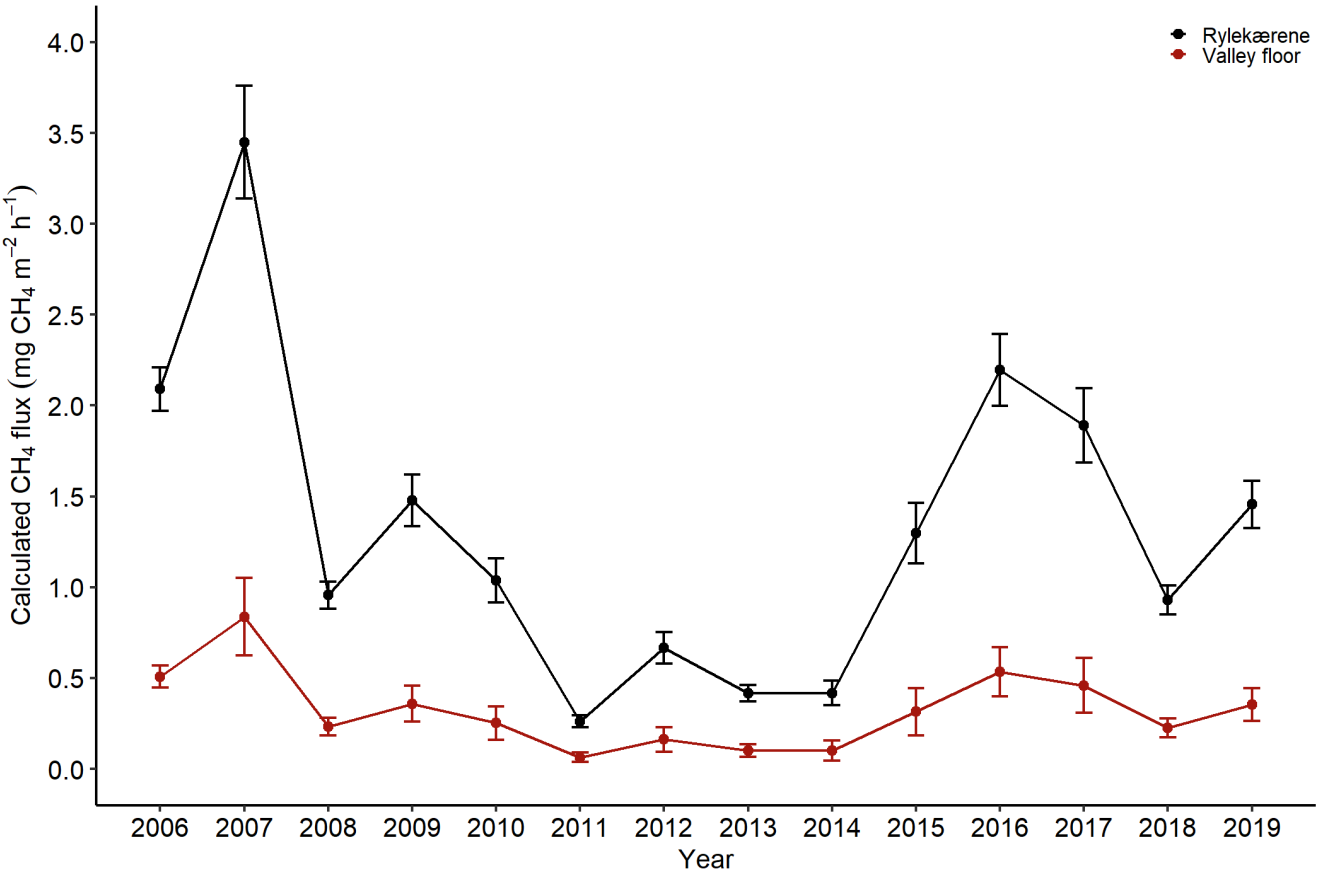

and chamber 6 at the AC site. ***Data sources: GEM ClimateBasis and GeoBasis Zackenberg.***

3.2 Timeline of methane fluxes from Rylekærene

Figure 4 summarizes the methane fluxes measured on fen and fen fringe (only AC 1 to 6) surface types in Zackenberg Valley during 17 growing seasons from 1997–2019. The methane fluxes vary both between simultaneous measurements and between years. Fen fluxes generally show higher fluxes than those measured at the fen fringe, with mean fluxes ranging from 1.75 ± 0.27 to 8.3 ± 0.31 mg m^{-2} h^{-1} in 1997 (Friborg et al., 2000)

and 2000 (Joabsson and Christensen, 2001). Methane fluxes in the fen fringe ranged from 0.26 mg ± 0.07 m^{-2} h^{-1} in 2011 to 3.41 ± 0.57 m^{-2} h^{-1} in 2007 during July–August (Mastepanov et al., 2013; Mastepanov et al., in prep.).

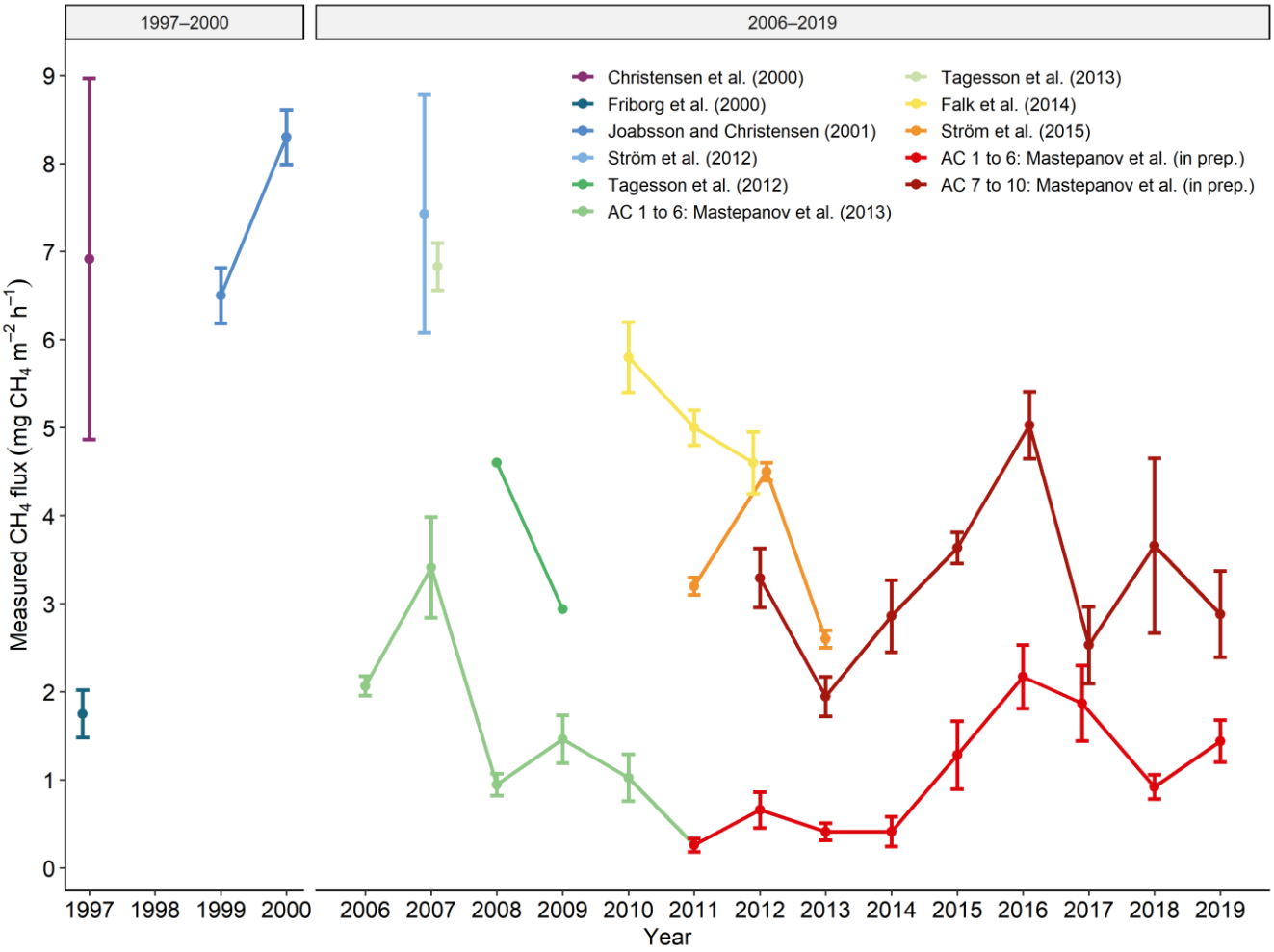

Figure ~~5: The calculated area-integrated July–August methane fluxes and SE for Rylekærene and the valley floor from 2006–2019.~~

~~3.5 Methane emissions from the valley in a changing climate~~

~~The mean valley methane flux for July–August is shown for 2008–2015, 2041–2060, and 2081–2100 (Fig. 6). For the two future periods, the mean fluxes are depicted as changed in an RCP8.5 scenario together with the sensitivity to surface erosion changes. The mean valley flux, excluding erosion, was 0.2 mg m^{-2} h^{-1} for 2008–2015, 0.32 mg m^{-2} h^{-1} for 2041–2060, and 0.45 mg m^{-2} h^{-1} for 2081–2100. The valley methane flux decreases when the eroded surfaces increase in areas with grasslands and fens. The conversion of areas with a methane uptake (Heath areas and *Salix* snowbeds) increases the valley flux. The net effect of the contributions to the mean valley flux from the~~

four surface types is negative, reducing the mean valley flux. The net reduction from erosion is −0.3 % and −1.6 % in the 2041–2060 period, increasing to a mean net reduction of −0.7 % and −7.8 % between 2081–2100.

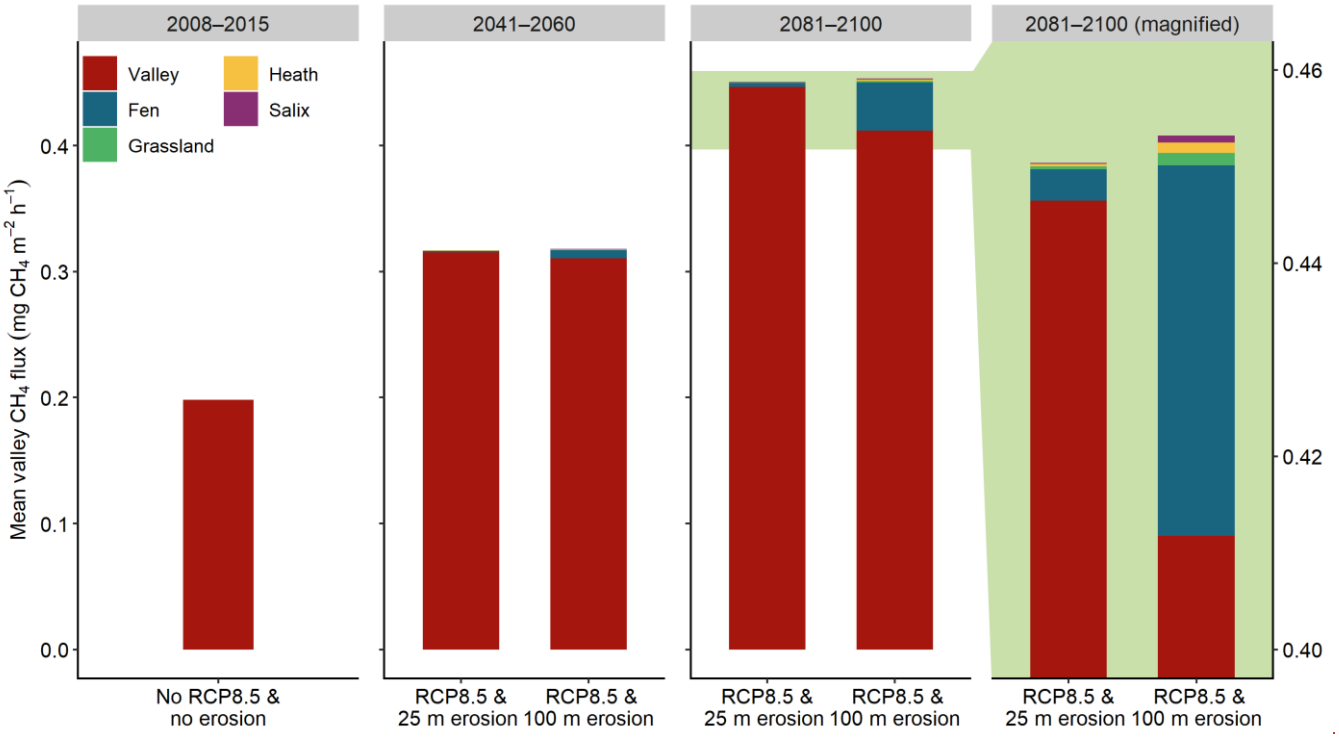

Figure 6: In the RCP8.5 scenario, the mean July–August valley methane flux increase over time, summarized here in two future periods, 2041–2060 and 2081–2100. Increases in flux from rising temperatures are partly offset by erosion in the sensitivity study. The increasing erosion of the four surface classes could change the mean flux of methane in the valley over time. While erosion of grasslands and fens act as relative methane sinks, some of that sink is counterbalanced by a relative source from the loss of *Salix* snowbeds and Heath areas.

4 Discussion

4.1 Methane studies in Zackenberg Valley

Methane flux has been the subject of several measurement campaigns in Zackenberg Valley since 1997. The length of these campaigns, their onset compared to the beginning of the growing season, the sampling area, and strategy varied between studies. Figure 7 shows a timeline of methane flux campaigns from published studies and data from the annually updated GEM database. The approximate locations of the measurement sites are shown in Fig. 2, and a summary of the mean methane fluxes is shown in Fig. 8. With the exemption of Tagesson et al. (2012), which reported mean fluxes specifically for the 2008–2009 growing seasons, the following mean values cover the length of the whole measurement period.

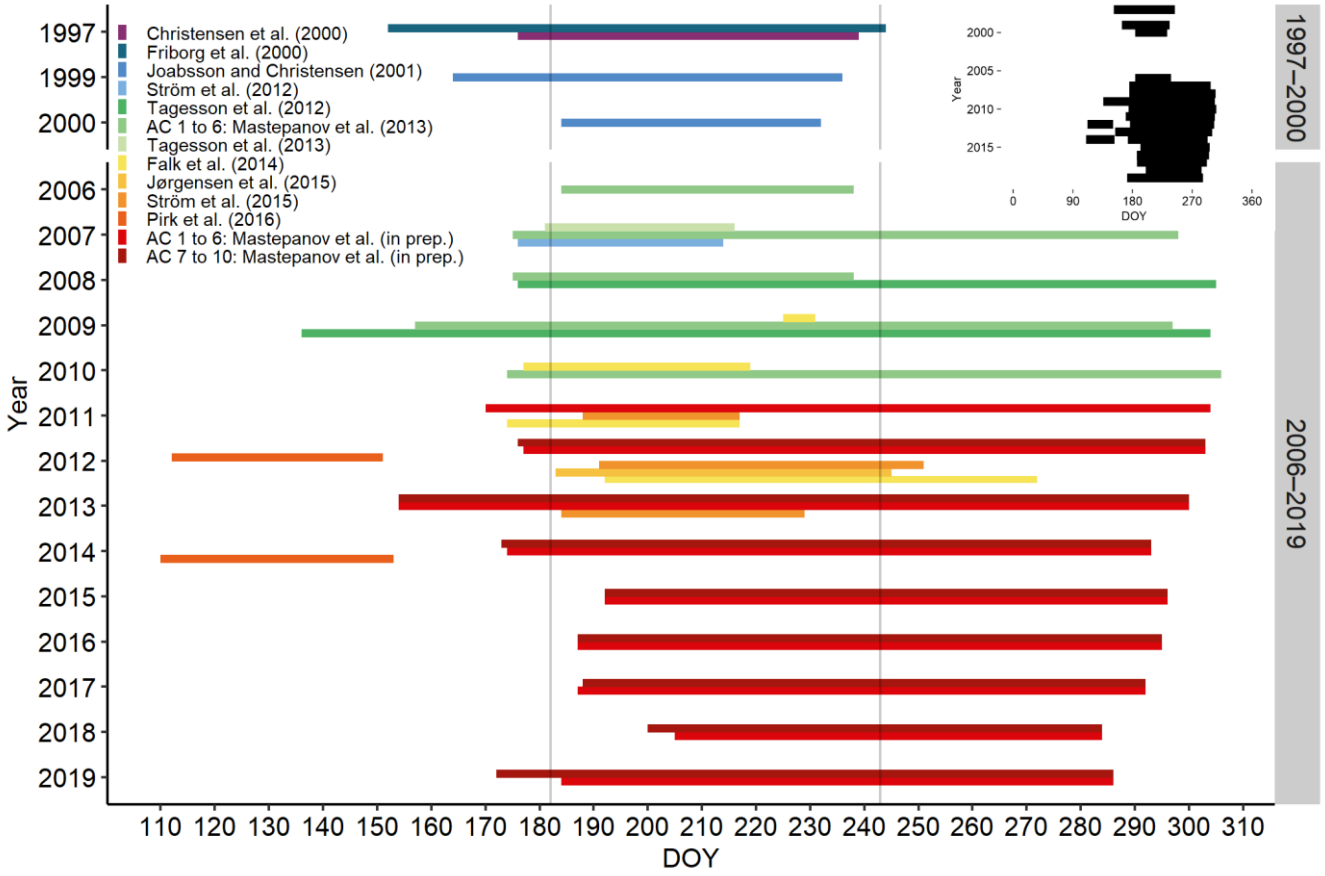

~~Figure 7:~~4. Timeline of methane fluxes measured during the growing season (1 July–31 August for AC) measured in ~~Zackenberg Valley, covering both~~ fen areas (hummocky and ~~area-integrated fluxes for Rylekærene~~continuous fen) and at the ~~valley floor.~~fringe of the fen (AC 1 to 6). Colors show different ~~publications, and marker shapes indicate the location. Please note that the years 2001–2005 are left out, as no published studies focusing on methane fluxes in undisturbed areas were made in this period. Also, note that points may be shifted slightly along the year axis to avoid overplotting.~~datasets

~~Using a distributed manual chamber approach, Christensen et al. (2000) measured a flux for an intensive study area, a part of Rylekærene, of 4.9 ± 0.6 (mean ± SE) mg m^{-2} h^{-1} in 1997. Friborg et al. (2000), using the EC method, found a methane flux for approximately the same area in the same year of 1.75 ± 0.27 mg m^{-2} h^{-1}, i.e., less than half the mean flux in Christensen et al. (2000). This difference was attributed to a higher proportion of drier areas in the fetch of the eddy tower. Using the Zackenberg vegetation map of Bay (1998), Christensen et al. (2000) used the flux measured at each of the surface cover types to calculate a mean valley flux of 1.9 ± 0.7 mg m^{-2} h^{-1}. Joabsson and Christensen (2001) measured methane flux at control plots for a plant treatment study in 1999 and 2000, near the southern boundary of Rylekærene. The mean methane flux was 6.5 ± 0.32 mg m^{-2} h^{-1} in 1999 and 8.3 ± 0.31 mg m^{-2} h^{-1} in 2000. Control plot data from a comparable experimental manipulation by Ström et al. (2012) gave a mean of 7.43 ± 1.35 mg m^{-2} h^{-1} near the current MM2 site. Mastepanov et al. (2013) published the first multiyear methane flux time series, covering the growing season four years from 2006–2010 at the AC site. These measurements continued in 2011–2019 (Mastepanov et al., in prep.). Data from the AC time series were reanalyzed for the 2006–2019 period, only taking fluxes in July–August into account. The mean of all measurements in the six chambers that have been operational through this entire period was 1.27 ± 0.01 mg m^{-2} h^{-1}. Four chambers were added in 2012, which extended the chamber measurements further out into the fen. These four chambers showed~~

~~generally higher methane fluxes, ranging from 1.95 ± 0.23 mg m^{-2} h^{-1} in 2013 to 5.03 ± 0.38 mg m^{-2} h^{-1} in 2016, and a mean flux of 3.36 ± 0.02 mg m^{-2} h^{-1} for the 2012–2019.~~

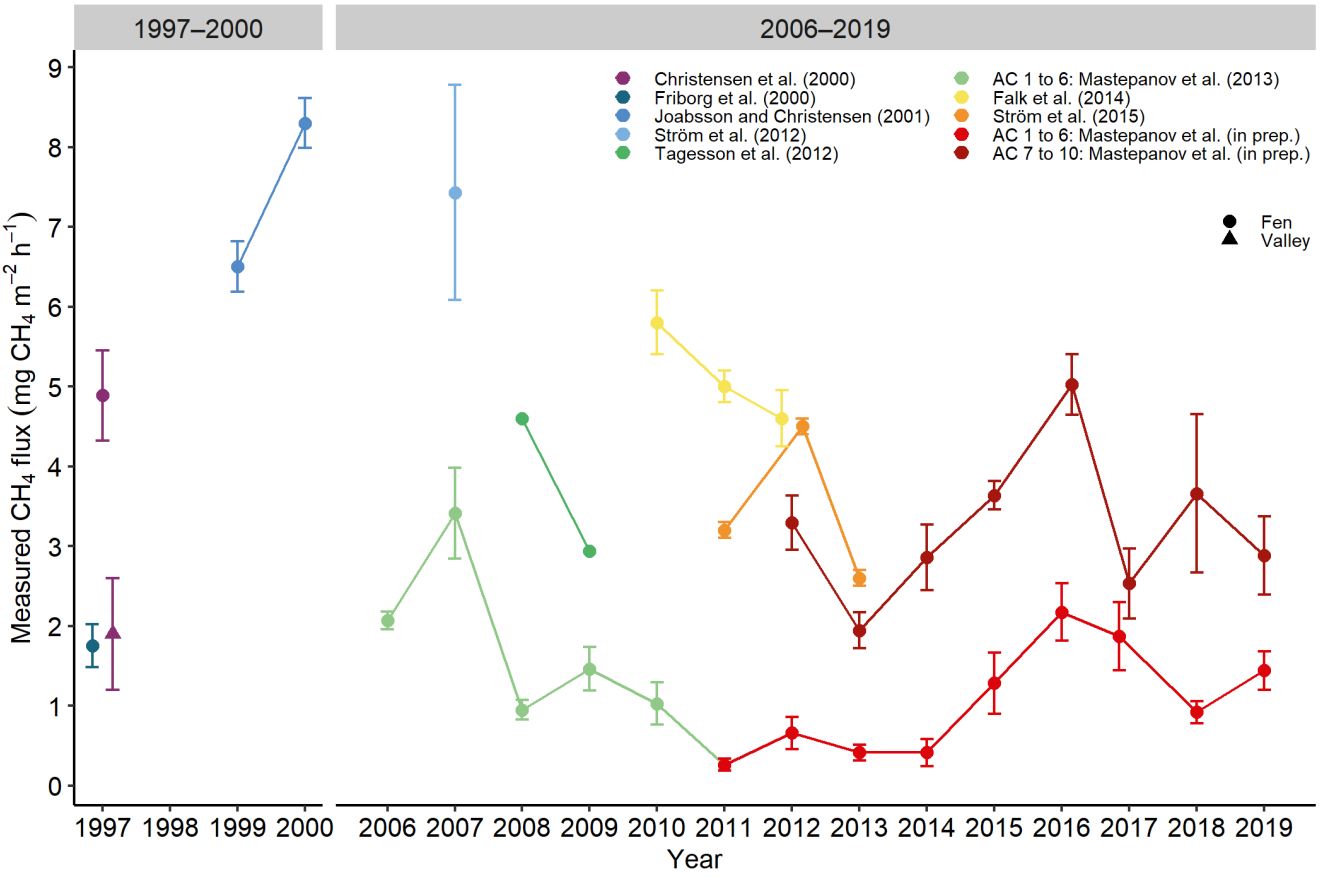

~~**Figure 8: Timeline of methane fluxes measured during the growing season (1 July–31 August for AC) in Zackenberg Valley, covering both fen areas and area-integrated fluxes for Rylekærene and the valley floor. Colors show different publications, and marker shapes indicate the location.**~~ **Please note that the years 2001–2005 are left out, as no published studies focusing on methane fluxes in undisturbed areas were made in this period. Also, note that points may be shifted slightly along the year axis to avoid overplotting.**

3.2 Gully methane fluxes

Methane fluxes at exposed, eroded surfaces of the gully were different from the fluxes on the nearby, undisturbed surfaces (Fig. 5). The late growing season mean methane flux of the recently eroded surfaces in the gully in 2019 was 0.05 ± 0.02 mg m^{-2} h^{-1}, including positive and negative fluxes. The grassland surface cover in areas not disturbed by erosion shows a negative methane flux of −0.06 ± 0.01 mg m^{-2} h^{-1}. The mean methane flux in the fen was 3.83 ± 0.76 mg m^{-2} h^{-1}, more than 75 times higher than the mean flux in the gully. For several plots in the fen, the flux was highly variable over time, reaching 20 mg m^{-2} h^{-1}. Generally, the methane flux decreased with air temperature in the fen. In the gully, plots with patches of live vegetation showed mostly negative flux, while barren plots exhibited a positive flux. In the undisturbed grassland areas, vegetated and barren plot fluxes were negative. Methane emissions generally increased closer to the open water body of the nearby fen. The emergence of the gully changed the area from a small methane sink to a small source, following an initial substantial episodic release of methane stored in exposed ice in 2018 when the gully appeared (Christensen et al., 2020b).

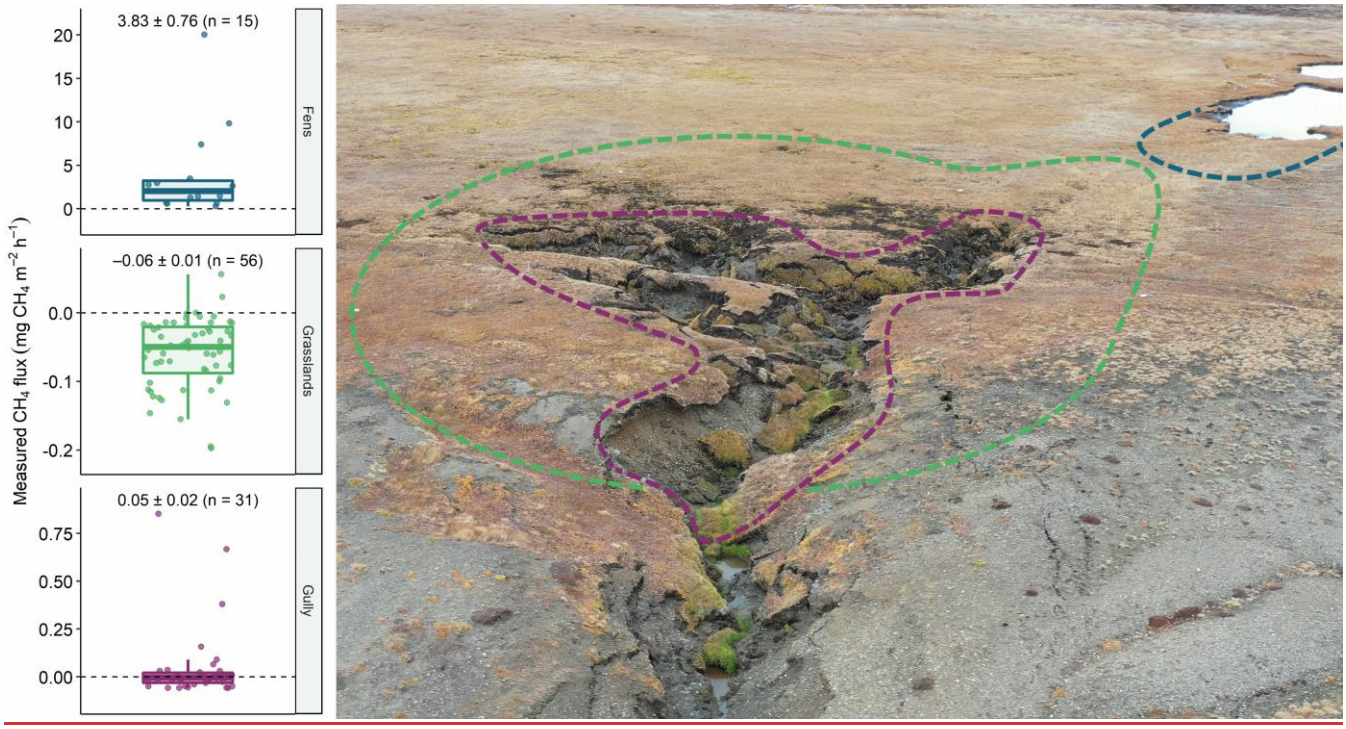

Figure 5. The gully and fen area near the Zackenberg Research Station. The three boxplots show the measured methane fluxes on different surface types between 23 August and 1 September 2019, when the image was captured. Dots on top of the boxplots show all the individual measurements. The dashed lines in the image indicate the approximate spatial extent of the measurements near the gully. The eroded area is ~50 m long and ~25 m at its widest, covering ~720 m^2.

3.3 Estimation of an integrated flux of methane in Zackenberg Valley

The July–August landscape flux of methane exposed large interannual variability over the valley floor and Rylekærene study areas over the 14 years, 2006–2019 (Fig. 6). The cumulative landscape fluxes and uncertainties are displayed as line plots and error bars overlapping stacked bar charts, which show the contribution from each of the six surface classes. Surface types with negative methane flux lower the landscape flux and SE for each of the surface classes on the stacked bar charts.

We observed no apparent trends for both areas (n = 14, *Pearson's* r = −0.22, p = 0.44) over the entire period. The mean flux for the 2006–2019 period in Rylekærene was 1.74 ± 0.16 mg m^{-2} h^{-1} and 0.34 ± 0.03 mg m^{-2} h^{-1} for the valley floor study area. Methane fluxes ranged from 0.98 ± 0.11 mg m^{-2} h^{-1} in 2011 to 3.26 ± 1.15 mg m^{-2} h^{-1} in 2007 in Rylekærene and from 0.17 ± 0.05 mg m^{-2} h^{-1} to 0.67 ± 0.23 mg m^{-2} h^{-1} for the valley floor. The two study areas were net sources of methane throughout the period, although its magnitude changed significantly between years.

Areas with a high positive flux are, in relative terms, more dominant in Rylekærene than the valley floor, which instead has a more considerable negative flux from heaths, *Salix* snowbeds, and fell and barren areas, which decrease the mean landscape flux.

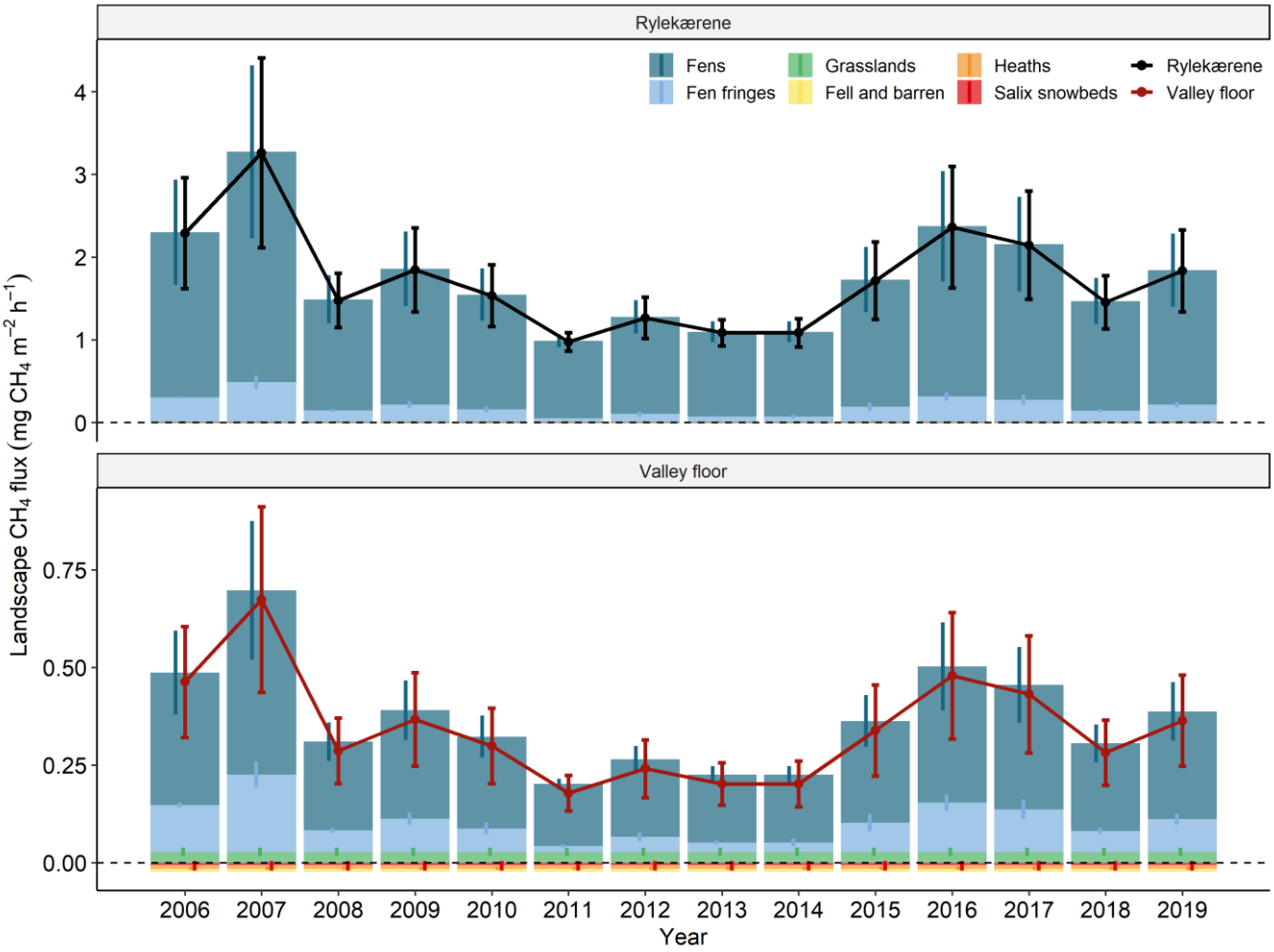

Figure 6. Cumulative fluxes and SE from the six surface classes are shown for the two areas. Fluxes and SE from each surface class are weighted to their relative coverage and shown with stacked bars.

3.5 Methane emissions from the valley in a changing climate

The mean valley methane flux for July–August is calculated for 2016–2100, including the upper and lower bounds for the fluxes, when uncertainties from both the methane-temperature regression and the upscaling are combined (Fig. 7). For this comparison, mean fluxes are averaged over two periods, one for the mid-21st century (2041–2060) and another for the late-21st century (2081–2100). The mean landscape flux in the reference period (2008–2015) was 0.27 mg m^{-2} h^{-1} (Fig. 7, a), while the mean flux from 2016–2019 (Fig. 7, b) was 0.39 mg m^{-2} h^{-1}. The modeled landscape flux without erosion (Fig. 7, c) increases linearly over the century. The modeled flux with erosion rates of 720 m^2 y^{-1} (Fig. 7, d), 720–3600 m^2 y^{-1} (Fig. 7, e), and 720–7200 m^2 y^{-1} (Fig. 7, f) all result in a net reduction in landscape flux, which becomes more pronounced over time. Higher rates of erosion result in lower modeled flux for Zackenberg Valley.

When considering the differences between the fluxes shown in Fig. 7, the mid-century mean landscape flux could be reduced by up to 0.05 mg m^{-2} h^{-1}, i.e., the difference between (Fig. 7, c) and (Fig. 7, f) corresponding to a

reduction of 1.2 % of the landscape flux. Between 2081–2100, the reduction in methane flux for the most severe erosion pathway could be 0.029 mg m^{-2} h^{-1}, equal to a reduction in the landscape flux of 4.9 %.

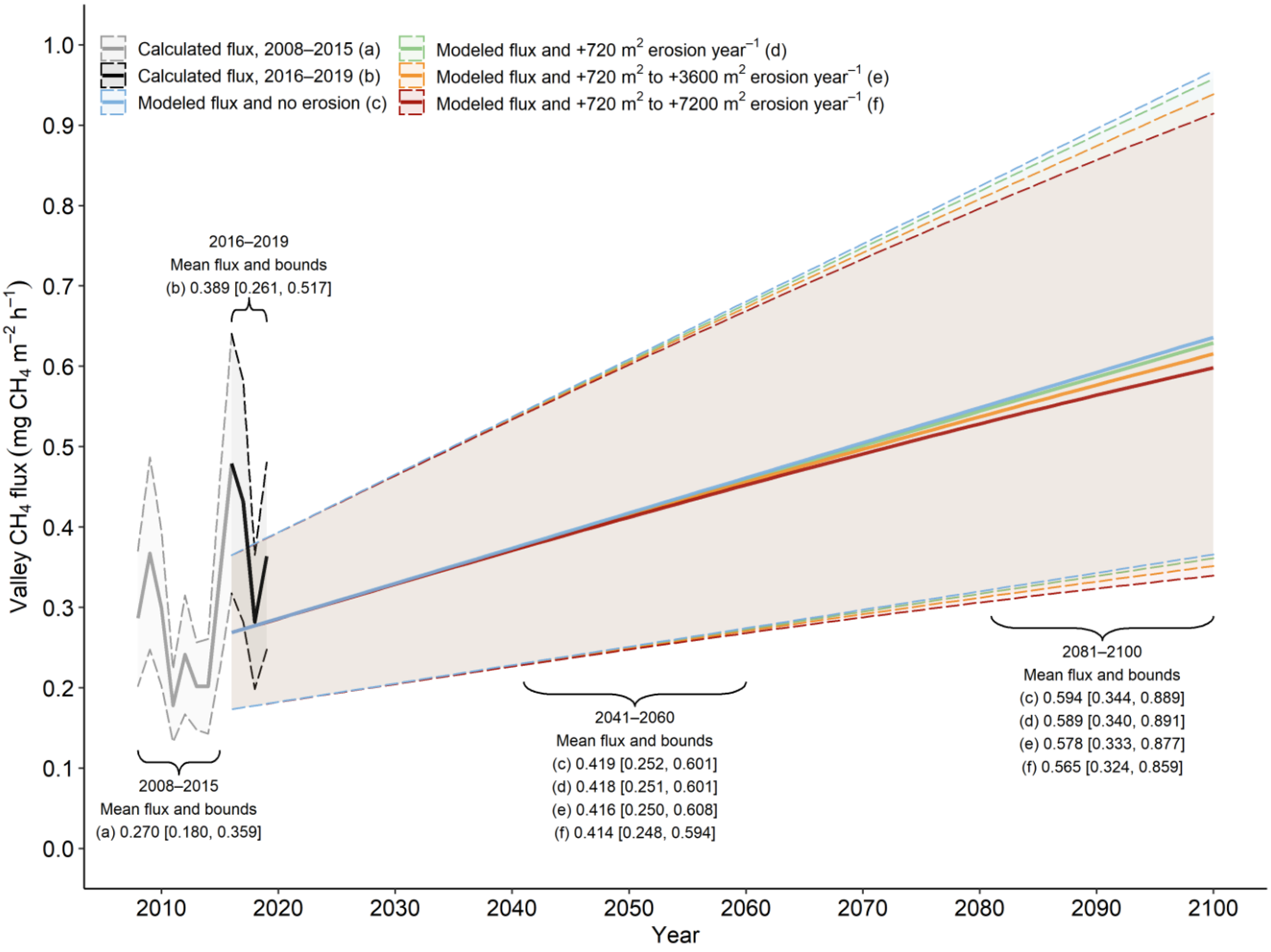

Figure 7. Methane fluxes in the valley floor study area increase over time if temperatures rise as modeled for the RCP8.5 scenario. However, increases in flux from rising temperatures are partly offset by erosion in the sensitivity study. Increasing erosion rates could reduce the mean flux of methane in the valley over time when a part of the landscape, a net source of methane, is converted into eroded areas with lower methane flux.

4 Discussion

4.1 Methane flux measurements

Several methane flux methods have been in use since the two first methane flux studies were carried out in 1997 (Fig. 4) in the Rylekærene area (Christensen et al., 2000; Friborg et al., 2000), including both manual chambers (Table 2) and EC measurements. Flux measurements over 14 years at AC show large interannual variability in methane fluxes even at a single site. Substantial spatial variability in fluxes is seen in Fig. 4 when studies are available in the same years. Differences in methane fluxes measured from these studies can be explained by site characteristics, equipment and sampling strategies, and both length and timing of the measurement period. Two studies are omitted in Fig. 4: Pirk et al. (2016b) studied the methane fluxes in the fen areas near the AC site under

snow-covered conditions before the growing season in 2012 and 2014. Jørgensen et al. (2015) added flux measurements from 2012 covering only 'dry tundra' (*Dryas* heath, abrasion plateau, and fell field) and 'moist tundra' (*Salix* snowbeds and *Cassiope* heath) sites, both of them methane sinks. These findings exceeded the methane uptake on similar tundra surface classes in the area in Christensen et al. (2000). Higher soil and air temperatures in 2012 compared to 1997 could explain the higher fluxes (Fig. 3a), which also fits with relatively high methane uptake in 2007 when Tagesson et al. (2013) did their measurements on corresponding vegetation types. Spatial differences and the inclusion of unvegetated surfaces (abrasion plateau and fell field) and more advanced measurement equipment (Table 2) are other possible reasons for the larger uptake in Jørgensen et al. (2015).

Using a distributed manual chamber approach, ~~Tagesson et al. (2012) estimated the integrated methane flux in Rylekærene at the current MM2 site (Fig. 2) using the gradient flux method for the growing season in 2008 and 2009. They found a flux of 4.6 mg m^{-2} h^{-1} and 2.94 mg m^{-2} h^{-1}, with alternative error reporting.~~

~~Based on measurements in the growing seasons 2010–2012, Falk et al. (2014) reported a mean methane flux of 5.8 ± 0.4 mg m^{-2} h^{-1}, 5.0 ± 0.2 mg m^{-2} h^{-1}, and 4.6 ± 0.35 mg m^{-2} h^{-1}, respectively, for 2010, 2011, and 2012 in untreated plots in Rylekærene. In this same northwestern part of Rylekærene Ström et al. (2015) used mobile flux chambers at multiple (16+) untreated plots and measured during three field campaigns in 2011, 2012, and 2013 a mean methane flux of 3.2 ± 0.1 mg m^{-2} h^{-1}, 4.5 ± 0.1 mg m^{-2} h^{-1}, and 2.6 ± 0.1 mg m^{-2} h^{-1}, respectively.~~

~~Three studies are omitted in Fig. 8: Pirk et al. (2016b) studied the methane fluxes in the fen areas near the AC site under snow-covered conditions before the growing season in 2012 and 2014. Jørgensen et al. (2015) added flux measurements from 2012 covering only dry tundra sites acting as a methane sink (*Dryas* heath, abrasion plateau, and fell field) and moist tundra (*Salix* snowbeds and *Cassiope* heath). These findings confirmed the atmospheric sink of the dry tundra heath, first reported by Christensen et al. (2000). Tagesson et al. (2013), which provide data for the landscape fluxes in this study, used a modeling approach for calculating a flux time series in Rylekærene covering 1997, 2000, 2002, and 2007–2010. Their study was based on both in situ flux measurements and modeling using environmental parameters and satellite imagery, meaning their results are not directly comparable to the in situ measurements shown in Fig. 8.~~

~~The~~Christensen et al. (2000) measured fluxes for an intensive study area, a part of Rylekærene, in 1997. In Fig. 4, only the combined measurements from hummocky and continuous fen plots are used. Alongside, Friborg et al. (2000) applied the EC method and found a much lower methane flux compared to Christensen et al. (2000) in approximately the same area. The fetch of the EC tower included surface classes with lower flux, which is a likely reason for lower mean flux Rylekærene reported in Friborg et al. (2000). The length of the measurement period was longer in Friborg et al. (2000), starting 1 June (Fig. 2), more than three weeks earlier than Christensen et al. (2000), which further explains some of the differences as methane fluxes were low at the beginning of the measurement period. Christensen et al. (2000) measured methane fluxes two times per week per plot, while

methane fluxes from EC were available every day for several weeks in July and August. The SE for the fen measurements in Christensen et al. (2000) in Fig. 4 is high due to the high flux variability within and between the two combined groups, hummocky and continuous fen.

Control plot flux measurements from Joabsson and Christensen (2001) are illustrated in Fig. 4 for a study site in the southern part of Rylekærene in 1999 and 2000. As shown in Table 2, the methods are comparable to Christensen et al. (2000), and the mean flux in both years is similar. The SE are smaller, likely due to both fewer and less diverse plots, i.e., six continuous plots compared to a total of 18 hummocky and continuous plots in Christensen et al. (2000).

Two studies provide a basis for comparison in 2007, the growing season with the highest estimated landscape flux in the 14-year study period. Ström et al. (2012) and Tagesson et al. (2013) applied similar methods (Table 2), using plots near MM2 in the same year with comparable methane flux as a result. For Ström et al. (2012), the SE reported in Fig. 4 is comparatively high. This difference can be explained by the high SE associated with measurements of plots with high flux and high *Eriophorum scheuchzeri* coverage, combined with relatively low methane flux plots with low *Eriophorum scheuchzeri* coverage. In Tagesson et al. (2013), measurements were done at 25 randomly-placed plots in hummocky and continuous fen areas, which resulted in a lower SE for the combined fen classes. The key difference is the range of both high and low *Eriophorum scheuchzeri* plots in Ström et al. (2012) against the randomly selected placement in two fen classes in Tagesson et al. (2013).

In 2008 and 2009, Tagesson et al. (2012) combined gradient and EC methods to estimate methane fluxes. Their results for the two growing seasons show intermediate fluxes between the fluxes measured at the fen fringe and higher fluxes measured by chamber methods on fen surfaces. The size of the fluxes can be explained by the limited 43 % coverage of the fen surface class in the tower footprint for the prevailing wind direction in the growing season, while the rest of the footprint is covered by drier surface classes. Error estimates are not directly comparable with the other studies in Fig. 4. They are integrated over the entire measurement period and reported as total accumulated errors equal to 8 % and 12 % of the total flux in 2008 and 2009.

Based on control measurements in a continuous fen area during the growing seasons 2010–2012, Falk et al. (2014) reported mean methane fluxes larger than those measured at the fen fringe at the AC. Measurement methods are comparable to Ström et al. (2012) and Tagesson et al. (2013). They use an identical gas analyzer and similar measurement frequency. Different chamber sizes are used, but this is not expected to impact the measurements significantly, as chamber volumes are considered in the calculation of fluxes. Differences in mean flux between the three years were attributed to variable measurement periods in the three years and interannual variations in water level depth (Falk et al., 2014).

Ström et al. (2015) measured methane fluxes with the same approach as Falk et al. (2014). The main differences between the two studies are the timing and the site. The two sites are situated ~600 meters apart, which explains possible differences in fluxes due to water levels and substrate availability. Measurements in 2011 in Falk et al. (2014) began 14 days earlier, which may have caused some of the difference in mean fluxes. In 2012, fluxes were similar between the two studies. The two campaigns started one day apart in that year, indicating that conditions are similar despite the distance.

The outer four chambers of the AC installation show interannual variability in fluxes of a size similar to the manual chamber measurements of Falk et al. (2014), Ström et al. (2015), and EC measurements in Tagesson et al. (2012). The number of observations for chambers 7 to 10 is high (Table 3), and flux measurements from each chamber are available every 90 minutes during July and August. In some years, measurements are not available for the entire period. Differences in chamber fluxes may be explained by variability in water levels, but data not available from the outermost chambers. Standard errors are higher due to relatively high variability in fluxes during the measurement period.

The previous studies show large differences in methane flux within the same fen ecosystem. Local spatial variability, interannual differences may explain these differences, and possibly also by differences in methods.

~~Spatial variability in methane flux can be pronounced in tundra ecosystems with complex microtopography (Olefeldt et al., 2013) and differ significantly even at a meter-scale (Fig. 3). Methane fluxes vary with local differences in substrate, water-table depth, grazing, and vegetation composition and productivity, each of which can either increase or limit the methane flux. Several of these interactions have been studied in Zackenberg Valley: increased substrate availability, mainly acetate, contributes to higher methane fluxes as shown by, e.g., Ström et al. (2003), while a low water table limits methane fluxes (Tagesson et al. (2013). Grazing can either increase (Falk et al., 2015) or decrease (Falk et al., 2014) the methane flux, depending on the vegetation cover. Vegetation composition and primary productivity are strong drivers of methane fluxes (Joabsson and Christensen, 2001; Ström et al., 2012; Ström et al., 2015).~~

Spatial variability in methane flux can be pronounced in tundra ecosystems with complex microtopography (Olefeldt et al., 2013) and differ significantly even at a meter-scale (Fig. 4). Methane fluxes vary with local differences in substrate, water-table depth, grazing, vegetation composition and productivity, each of which can either increase or limit the methane flux. Several of these interactions have been studied in Zackenberg Valley: increased substrate availability, mainly acetate, contributes to higher methane fluxes as shown by, e.g., Ström et al. (2003), while a low water table limits methane fluxes (Tagesson et al., 2013). Grazing can either decrease (Falk et al., 2014) or increase (Falk et al., 2015) the methane flux, depending on the vegetation cover. Vegetation composition and primary productivity are strong drivers of methane fluxes (Joabsson and Christensen, 2001; Ström et al., 2012; Ström et al., 2015).

Temporal variability in methane fluxes can be caused by differences in environmental parameters, both within a growing season and from one year to another. Soil temperature was found to explain less variability than species

composition and primary productivity ~~(Christensen et al., 2000; Ström et al., 2012),~~(Christensen et al., 2000; Ström et al., 2012), while soil temperatures showed a high correlation with methane flux within most individual years ~~(Mastepanov et al., 2013).~~(Mastepanov et al., 2013). Late-lying snow delays the beginning of the growing season ~~(Grøndahl et al., 2008),~~(Grøndahl et al., 2008), which controls several of the above-mentioned parameters ~~mentioned above.~~ Only a few studies in Zackenberg Valley were conducted outside the growing season. However, the fall season could substantially impact the annual methane budget, mainly through emissions associated with the onset of soil freezing ~~(Mastepanov et al., 2008).~~(Mastepanov et al., 2008). In contrast, wintertime (November–May) ~~emission~~emissions may only have a limited impact on the annual methane budget ~~(Pirk et al., 2016b).~~(Pirk et al., 2016b).

Our analysis focuses on the mean of the July–August fluxes in the valley, but the automated chambers are running from snowmelt to the end of the field season (Fig. ~~7~~2). The fixed period matches the timing of the previous studies, and the period showed a good representation of the mean flux of the entire measurement dataset. The first 30 to 40 days after snowmelt have been shown to express the main differences between years ~~(Mastepanov et al., 2013),~~(Mastepanov et al., 2013), which is covered by the July–August ~~means~~mean fluxes to a large extent.

4.2 ~~Landscape~~Combining flux measurements from multiple sources

Comparable mean methane fluxes across several existing studies indicate that the differences in methods and placement have an impact on the flux in fen areas. Differences arise mainly when measurement periods vary by several weeks and when measurement plots are distributed over several different surface classes, i.e., hummocky and continuous fen. However, the fen fringe time series appears to express some of the variability in fluxes as the separate measurement campaigns when these are combined into one. Regression analysis shows a significant correlation between methane fluxes at chambers 1 to 6 and the grouped studies from the fen areas of Zackenberg Valley when pairing data for the same years. Deming regression is a reasonable choice of analysis when both the mean values of chamber 1 to 6 and the fen methane fluxes are associated with measurement errors and uncertainties. The composite fen dataset, made from six separate studies, increases the temporal coverage and the spatial coverage of the data used in the regression analysis. The SE of the calculated fluxes is estimated with jackknife resampling, providing a reasonable SE estimate for Deming regression (Linnet, 1990). When comparing flux data to OLS regression, the Deming regression slope is steeper. The steeper slope means that the estimated fen flux in 2007, when the flux was high, is ~20 % higher when compared to OLS, which means that the difference in regression methods has a substantial impact on landscape fluxes.

~~The AC site is located by the outlet of the Rylekærene fen. The substantial flow of water through the area affects the water level, particularly at the innermost six chambers, which are located along the slight topographic gradient at the fen fringe. The changing water level may control the methane flux and explain its high variability 2006–2019, but neither the water levels, the air, nor soil temperatures correlate significantly (p value threshold of 0.05) with methane when analyzing the interannual variability for July–August mean values. Over the 14 years, p values range from 0.29 to 0.56. The lack of correlation over the time series illustrates a complex interaction between methane and environmental conditions when analyzed on a decadal scale. Figure 8 shows the methane flux of~~

~~previous studies, which have mainly focused on wetter parts of the fen where the flux is high. The flux appears to vary relatively less over time further out in the fen, as the soil moisture conditions change less between years than the chambers 1 to 6 at the AC site. One example is the smaller relative variability at chambers 7 to 10. The sizeable interannual variability shown in Fig. 3 could be more common for the smaller, discontinuous fen areas in the valley seen in Fig. 2. These areas are characterized by a less stable inflow of water than Rylekærene, which may therefore cause high interannual variability in the transition zones between different vegetation types.~~

Methane fluxes measured in chambers 1 to 6 are consistently lower than the fluxes in chambers 7 to 10. Therefore, data from chambers 1 to 6 are split into a separate surface class, the fen fringe. The addition of these lower flux fen areas impacts the landscape flux, but the width of the zone does most likely fluctuate across the valley. Here, 10 m is a simple estimate based on the situation at AC, but the width of the zone ultimately depends on the topographic gradient along the edge of the fens.

The remaining surface classes contribute with the same negative fluxes throughout the period, with a mean value representing each of the surface classes. Their net effect is offsetting some of the positive landscape methane flux, particularly for the valley floor. Several surface classes were studied in detail over a single growing season (Table 3), and the specific sites differ between studies. The fluxes from these areas are held constant in lack of more detailed data, and fluxes from different studies are averaged into a single mean flux, which represents a range of sites and environmental conditions. We omitted surface flux data from the grasslands, measured by Christensen et al. (2000). The measured mean flux was significantly higher at 2.1 ± 1.6 mg m^{-2} h^{-1}, and the measurement site was located near the border of the fen, see Fig. 2 in Christensen et al. (2000), making the data more comparable to the fen fringe than the grasslands surface class.

Manual measurements in the gully area were limited to 10 days in the late growing season. Still, the size of the mean fluxes is in good agreement with the concurrent fluxes measured at AC 7 to 10 (Mastepanov et al., in prep.) and the grassland flux reported in Tagesson et al. (2013). Negative fluxes were measured on plots with patchy vegetation in the gully, while mineral-rich plots had low positive fluxes of methane. The highest methane emissions in the gully were found on two unvegetated plots, located where the gully had recently eroded (up to 0.85 mg m^{-2} h^{-1}). These sparse observations suggest a considerable reduction in flux on eroded gully surfaces over time when limited organic soils remain in the gully.

4.3 Methane flux upscaling

Vegetation plot measurement on the dominant vegetation classes ~~in 2007~~ combined with long-term AC site data from 2006–2019 enables the calculation of landscape flux time series for Rylekærene and the valley floor. This approach is more direct than modeling based on physical parameters that have otherwise been shown to correlate well with methane flux for Rylekærene ~~(Tagesson et al., 2013).~~(Tagesson et al., 2013). However, a limitation of the approach is its lack of a dynamic component, which could take spatial differences across the valley into account,

e.g., snow cover or changing soil moisture conditions from one year to another, affecting the valley floor and the AC site differently.

~~Tagesson et al. (2013)~~Both Christensen et al. (2000) and Tagesson et al. (2013) found a significant difference in the methane flux in hummocky and continuous fen areas in Rylekærene and treated the two groups separately. These groups were combined in this study to match the existing~~,~~ valley-wide surface cover classification. Comparing the mean flux ~~in~~found for Rylekærene ~~over approximately the same period~~ shows good agreement between the flux estimates in this study and the ~~flux in Tagesson et al. (2013).~~fluxes reported in Tagesson et al. (2013). Four growing seasons (2007–2010) are common for the two studies, and in three ~~years~~of the seasons, the flux estimates of this study lie within the model uncertainty in ~~Tagesson et al. (2013).~~Tagesson et al. (2013). The one notable exemption is ~~the~~ 2007 mean flux (3.~~45 ± 0.31~~26 ± 1.15 mg m^{-2} h^{-1}) in this study, and it differs a lot from the 1.6 ± 1.0 mg m^{-2} h^{-1} modeling result~~.~~ in Tagesson et al. (2013). The difference can be explained with a relatively high flux measured at the AC site in a year without extreme temperature or moisture conditions in the valley (Fig. ~~1~~2), which are central parameters in the modeling of ~~Tagesson et al. (2013).~~ Tagesson et al. (2013).

The AC site is located by the outlet of the Rylekærene fen. The flow of water through the area affects the water level at the site, which is shown in Fig. 3d. Water level data was measured manually, once per day in the growing season, between 2006–2019 near the outermost of the six original chambers (chamber 1). Automatic water level measurements are available for chamber 1 and chamber 6, the innermost chamber, in the 2010–2019 period, with a gap in data for 2013. For July–August, water levels are generally lower at the innermost chamber but show variability similar to the water levels measured further out in the fen. Water level measurements are not available for the outer four chambers.

The changing water level may control the methane flux and explain its high variability 2006–2019, but neither water levels, air temperatures, nor soil temperatures correlate significantly (*p*-value threshold of 0.05) with methane when analyzing the interannual variability for July–August mean values. Over the 14 years, *p*-values range from 0.29 to 0.56. The lack of correlation over the time series illustrates a complex interaction between methane and environmental conditions when analyzed on a decadal scale. Figure 4 shows the methane flux of previous studies, which mainly focused on wetter parts of the fen where the flux is high. The flux appears to vary relatively less over time further out in the fen, as the soil moisture conditions change less between years than the chambers 1 to 6 at the AC site. One example is the smaller relative variability at chambers 7 to 10. Similar, large variability could common for the smaller, discontinuous fen areas in the valley seen in Fig. 2. These areas are characterized by a less stable inflow of water than Rylekærene, which may therefore cause high interannual variability in the transition zones between different vegetation types.

~~Christensen et al. (2000)~~Christensen et al. (2000) based their study of Zackenberg Valley methane flux on chamber measurements from a ~~c.~~ ~0.1 km^2 area of the northern part of Rylekærene (Fig. ~~2~~1). The methane flux was measured with chambers on the five dominant vegetation types, and a mean flux for the valley was calculated by scaling fluxes to match the land cover classification of ~~Bay (1998).~~Bay (1998). The upscaled methane flux for the entire

valley floor was 1.9 ± 0.7 mg m^{-2} h^{-1}, which is higher than in any of the years in this study ~~(~~, which range from 0.~~06~~18 ± 0.~~03~~05 mg m^{-2} h^{-1} and 0.~~84~~67 ± 0.~~21~~24 mg m^{-2} h^{-1}~~).~~. The distribution of land cover classes differs slightly between ~~Bay (1998)~~Bay (1998) and the HyMap dataset~~, which explains only some of the differences. However~~. Still, a primary cause for the much higher valley estimate is the higher measured fluxes in the widespread ~~Grassland~~grassland class with a flux of 2.9 ± 1.6 mg m^{-2} h^{-1} in ~~Christensen et al. (2000),~~Christensen et al. (2000), compared to 0.1 ± 0.04 mg m^{-2} h^{-1} (SE converted from SD) in ~~Tagesson et al. (2013).~~Tagesson et al. (2013), the source of the grassland flux data used in our study. This difference impacts the valley flux, and if we substitute only the ~~Grassland-~~grassland-type flux from 0.1 mg m^{-2} h^{-1} to 2.9 mg m^{-2} h^{-1} in the upscaling to the entire valley floor, it would ~~nearly~~at least double the methane flux in the valley. ~~The substantial difference could indicate that grasslands in the marginal zones of fens have substantially elevated flux of methane in wet years and, hence, are key players in valley-wide interannual methane flux variability.~~

~~Jørgensen et al. (2015) found a relatively high methane uptake on dry tundra, e.g., *Salix* snowbeds and Heath surfaces, compared to what has been found earlier. Including the uptake from Jørgensen et al. (2015) would further limit the valley flux or even make the valley a net sink of methane in dry, warm years, as these surface classes combined account for more than 40 % of the valley floor (Table 2). As a result, the magnitude of the fluxes in Fig. 5 may be underestimated, as both positive and negative fluxes from Tagesson et al. (2013) are lower than found in both Christensen et al. (2000) and Jørgensen et al. (2015). Additionally, the year 2007 was chosen for the comparison because it exists in both datasets. However, the methane flux was exceptionally high in that year (Fig. 3), which means that all other years in the time series were attributed to a lower flux. The valley methane fluxes are highly variable between years and do not show an increasing trend from the available data. Zackenberg Valley shows the potential for increased methane fluxes in the 21st century, as methane shows a positive correlation with temperatures which are expected to increase under the RCP8.5 climate scenario (Geng et al., 2019), similar to the trend of the rest of Greenland and the Arctic (AMAP, 2017).~~

Jørgensen et al. (2015) found a relatively high methane uptake on dry tundra in 2012, e.g., *Salix* snowbeds and Heath surfaces, compared to what has been found earlier. When including the uptake from Jørgensen et al. (2015), the valley flux is reduced, but the effect could vary between years with larger sinks in dry, warm years, as these surface classes combined account for more than 40 % of the valley floor (Table 1). Soil temperatures were lower in 2012 than in 2007 in July-August, which does not explain the higher uptake on dry tundra soils in 2012, indicating that some dry tundra surfaces have a higher methane uptake than others. Additionally, flux data from 2007 are used for both heath, grassland, and *Salix* snowbeds surface classes. While flux measurements in the fen areas were exceptionally high in that year, this was not the case for the drier surface types. Landscape fluxes from both the valley floor and Rylekærene are highly variable between years and do not show an increasing trend from the available data. Both study areas show the same pattern, but the areal distribution between classes differs, making the Rylekærene study area almost entirely dependent on the variability of only the fen and fen fringe surface types. In the larger valley floor study area, grassland, *Salix* snowbeds, heaths, and fell and barren surface classes dampen the variability between years.

Zackenberg Valley shows the potential for increased methane fluxes in the 21st century, as methane shows a positive correlation with temperatures (Geng et al., 2019), similar to the rest of Greenland and the Arctic (AMAP, 2017).

4.4 Methane flux upscaling in Arctic landscapes

Landscape-scale methane flux estimations are available from other subarctic and tundra sites (Table ~~3~~4) in North America, Scandinavia, and Russia. The upscaled growing season fluxes range from 0.5 km^2, extending from covering a few different ecosystems in a single site ~~(Christensen et al., 2004) to large-scale estimates of fluxes covering up to 320,000 km^2 for the Hudson Bay Lowlands (Roulet et al., 1994).~~(Christensen et al., 2004) to large-scale estimates of fluxes covering up to 320,000 km^2 for the Hudson Bay Lowlands (Roulet et al., 1994). Mean methane fluxes in these landscapes range from 0.3 to 3 mg m^{-2} h^{-1} across different scales and landscape types, covering growing seasons of variable length with studies scattered across several decades. The mean methane flux for Zackenberg Valley from 2006–2019 is 0.~~32~~34 mg m^{-2} h^{-1} in the valley floor area (~16 km^2) and 1.~~32~~74 mg m^{-2} h^{-1} in the fen-rich Rylekærene area (~1.3 km^2). Hence, the results from Zackenberg Valley are in good agreement with observations from comparable studies at other sites. However, the two Zackenberg study areas are smaller than most studies listed in Table ~~3~~4. All the included studies are either fully or partly based on chamber measurements and upscaling with areal coverage of the surface classes, making them comparable to this study. ~~Several of the studies (Bartlett et al., 1992; Roulet et al., 1994; Bosse and Frenzel, 2001; Hartley et al., 2015)~~Several studies (Bartlett et al., 1992; Roulet et al., 1994; Bosse and Frenzel, 2001; Hartley et al., 2015) estimated the landscape methane fluxes based on observations from a single year. The remaining studies combine observations from multiple years or studies to a flux estimate from each surface cover class ~~(Christensen et al., 2004; Schneider et al., 2009; Andresen et al., 2017; Morozumi et al., 2019).~~(Christensen et al., 2004; Schneider et al., 2009; Andresen et al., 2017; Morozumi et al., 2019). Flux measurements from several years lead to more robust landscape flux estimates, as the fluxes are highly variable between years~~, as the present study also shows~~.

The large differences in study area size and composition ~~are~~ ultimately ~~determining~~determine the mean methane flux estimates of the landscape, ~~which makes~~making direct comparisons between sites difficult. For instance, the mean landscape flux found in this study is nearly ~~four~~five times greater for the fen-rich Rylekærene study area, which is ~~entirely~~fully contained in the valley floor study area. On an even larger scale, the entire northeast Greenland acts as a net sink of methane, as ~~Jørgensen et al. (2015)~~Jørgensen et al. (2015) found a mean methane flux of ~−0.08 mg m^{-2} h^{-1} in their 10,675 km^2 study area.

Table ~~3:~~4. Comparison of landscape-integrated growing season methane flux for various subarctic and Arctic sites with a minimum size of 0.5 km^2.

Publication	Location	Climate zone	Landscape type	Mean flux (mg CH_4 m^{-2} h^{-1})	Area size (km^2)
~~Bartlett et al. (1992)~~Bartlett et al. (1992)	Yukon-Kuskokwim Delta (Alaska, USA)	Subarctic	Wetlands	1.8	97,400
~~Roulet et al. (1994)~~Roulet et al. (1994)	Hudson Bay Lowlands (Ontario-Manitoba, Canada)	Subarctic	Wetlands	0.8	320,000

~~Bosse and Frenzel (2001)~~Bosse and Frenzel (2001)	Yenisey River (W Siberia, Russia)	Subarctic	Mire, wetlands, and Pine forest	1	361
~~Christensen et al. (2004)~~Christensen et al. (2004)	Stordalen (Norrbotten, Sweden)	Subarctic	Mire	2.7 to 3.0	0.5
~~Heikkinen et al. (2004)~~Heikkinen et al. (2004)	Lek Vorkuta (N Komi, Russia)	Arctic tundra	Heath, peatland, and Salix	0.6	114
~~Schneider et al. (2009)~~Schneider et al. (2009)	Lena Delta (N Siberia, Russia)	Arctic tundra	Wetlands	0.4	29,036
~~Hartley et al. (2015)~~Hartley et al. (2015)	Kevo (Lapland, Finland)	Subarctic	Aapa mires and birch forest	0.3 to 0.4	100
~~Andresen et al. (2017)~~Andresen et al. (2017)	Utqiaġvik Peninsula (Alaska, USA)	Arctic tundra	Arctic coastal plains	0.6	1779
~~Morozumi et al. (2019)~~Morozumi et al. (2019)	Indigirka (NE Siberia, Russia)	Arctic tundra	Larch forest, shrubs, and wetlands	1.6	96

Several other studies have applied the EC method for ecosystem methane flux measurements ~~at~~on a landscape ~~-~~ scale in the Arctic, e.g., ~~Fan et al. (1992); Sachs et al. (2008); Wille et al. (2008); Jackowicz-Korczynski et al. (2010); Parmentier et al. (2011); Taylor et al. (2018).~~Fan et al. (1992); Sachs et al. (2008); Wille et al. (2008); Jackowicz-Korczynski et al. (2010); Parmentier et al. (2011); Taylor et al. (2018). While the EC method requires less workload and integrates ecosystem fluxes at high temporal resolution by nonintrusive means ~~and is preferred for these reasons,~~(McGuire et al., 2012), those studies are generally restricted to smaller areas less than 0.5 km^2. Ecosystem fluxes from these studies range between ~0.1 to 6.2 mg m^{-2} $h^{-1,}$ with the lowest growing season fluxes measured at an upland tussock tundra site by Eight Mile Lake in Alaska ~~(Taylor et al., 2018) and the highest fluxes measured in a mire in Stordalen, north Sweden (Jackowicz-Korczynski et al., 2010). Mean growing season fluxes found in Zackenberg using the EC method are within this interval (Friborg et al., 2000; Tagesson et al., 2012).~~(Taylor et al., 2018) and the highest fluxes measured in a mire in Stordalen, north Sweden (Jackowicz-Korczynski et al., 2010). Mean growing season fluxes found in Zackenberg using the EC method are within this range (Friborg et al., 2000; Tagesson et al., 2012).

4.~~3~~5 Landscape methane flux in a changing climate

A warming trend in both air and soil temperatures has been observed for Zackenberg Valley ~~(Abermann et al., 2017; Christensen et al., 2020b).~~(Abermann et al., 2017; Christensen et al., 2020b). The increase in temperatures has contributed to the destabilization of permafrost, leading to several active periglacial landforms in recent years ~~(Docherty et al., 2017; Cable et al., 2018; Christensen et al., 2020b).~~(Docherty et al., 2017; Cable et al., 2018; Christensen et al., 2020b). Modeling results show higher soil temperatures and a deepening of the AL in Zackenberg in the future ~~(Christiansen et al., 2008; Westermann et al., 2015).~~(Christiansen et al., 2008; Westermann et al., 2015). Increasing temperatures are expected to impact both positive and negative methane flux and surface erosion in the Arctic ~~(Geng et al., 2019; Schuur et al., 2015),~~(Schuur et al., 2015; Geng et al., 2019; Oh et al., 2020), which is also likely for Zackenberg Valley. The emergence of several active erosion sites ~~along the~~in Zackenberg ~~River~~Valley in recent years could be an initial step towards increased erosion activity ~~in~~during the 21st century ~~in~~

~~the valley.~~. In 2019, after the disappearance of methane-rich ice ~~-~~wedges in the previous year, carbon-rich soils had been washed out from the gully, leaving a silt-organic mix with limited potential for methane emission in the area ~~(Christensen et al., 2020b). This~~ (Christensen et al., 2020b). Our study defines ~~two~~three erosion ~~scenarios~~pathways to illustrate the sensitivity of methane flux to land cover changes on a valley ~~-~~scale. We hypothesize large-scale linear growth in eroded areas ~~along the banks of the Zackenberg River by the late 21st century (i.e., 2081–2100), characterized by the changes in fluxes like~~in parts of the valley that are likely to have a high ground ice content and are located near streams and rivers identified by Cable et al. (2018). These erosion areas are assumed to share the characteristics of those observed in the gully area in 2019. Increased gully erosion ~~would~~could transform large areas with ~~limited~~surfaces with both methane emission and uptake into well-drained, low emission eroded surfaces. These ~~two~~ erosion ~~scenarios~~pathways are unlikely~~,~~ but they are valuable as a sensitivity study illustrating the difference in importance of increasing temperatures relative to eroding surfaces. ~~In this example, a backward gully erosion area was studied, but erosion caused by the Zackenberg River, and especially GLOFs, appear to have a larger impact on the erosion of the riverbanks (Tomczyk et al., 2020) and would most likely have a similar effect on methane fluxes. Further, erosion of the riverbanks is more pronounced on the outer banks of the river bends (Tomczyk et al., 2020). Backward gully erosion may be limited to ice-rich parts of the riverbanks, but the extent of these is largely unknown along the Zackenberg River inside the study area (Cable et al., 2018).~~

Even large-scale erosion ~~along~~on the ~~river~~valley floor would have a limited impact on the mean ~~valley~~ methane flux, reducing ~~the flux~~it by ~~less than~~up to 1.2 % on average between 2041–2060~~, while surface erosion gradually progresses toward the first third of 25 m or 100 m, respectively.~~ for the most extreme erosion pathway (Fig. 7, f). The reduction becomes more pronounced (4.9 % reduction) between 2081–2100, as eroded areas would ~~develop further inland and cause disturbances to areas dominated by fen. When fen areas are eroded, the flux is expected~~continue to ~~decline, causing the area~~ erode at a faster pace. Disturbances of this magnitude are comparable to ~~become a relative sink of methane. The erosion could cause the mean methane fluxes of the~~ the size of the edge trimming during the GLOF in 2017 in the lower river section (Tomczyk et al., 2020), located inside the valley floor study area. The impact on fluxes from one added gully, similar in size to ~~decrease by −0.7 %~~the recent gully per year, is minimal (less than 1 % reduction) at the end of the 21st century (Fig. 7, d) when compared to the uncertainty range. In our calculation of landscape methane fluxes after erosion, eroded areas become revegetated at a rate of 2 % y^{-1}. This rate may change over time and ~~−7.8 % in the late period, with 25 m~~from one location to another, dependent on species composition and ~~100 m~~soil conditions in the eroded areas ~~along the river~~. The change is assumed to be linear in this case but may accelerate over time, as plant communities established. In the calculation, revegetated areas were considered to have the same methane flux as the grasslands in the gully area. Limited data from the measurements in the gully area shows that the undisturbed vegetated areas take up slightly more methane than the disturbed vegetation patches in the gully, but the 10-day measurement period did not allow for more detailed measurements on temporal dynamics in the area.

The resulting changes in flux following erosion, particularly for the less extreme pathways (Fig. 7, d and e), are minor relative to the considerable uncertainty in the general shift in methane for the valley following an increase in temperature. The mean methane flux is shown in Fig. 7 with a wide uncertainty range, partly caused by a lack of perfect fit between fluxes and temperatures and the uncertainties in the estimated landscape fluxes in Fig. 6. The variability between years in this study is substantial. The mean valley flux for 2016–2019 exceeds the confidence bounds, which shows that this should be seen as a sensitivity study of changes occurring on decadal scales.

In this case, methane fluxes were measured in a gully, which becomes more drained with a loss of organic soils from the surface after an erosion event ~~(Christensen et al., 2020b). Fluvial erosion of vegetated riverbanks would most likely have a similar impact on methane fluxes when organic soils and vegetation are eroded.~~(Christensen et al., 2020b).

The gully described in this study has likely formed as a direct consequence of pronounced lateral erosion from the river, which steepened the gully, allowing for increased drainage of water and sediments. The increased drainage exposed more and more of the ice -wedges and frozen soils, which later thawed and flowed out through the steeper gully. Lateral erosion of a similar scale has not been recorded to occur along the smaller rivers and streams in Zackenberg, but several smaller erosion sites have been described in recent years (Docherty et al., 2017; Cable et al., 2018). The gully shares characteristics with thermokarst gullies, a common type of thermokarst erosion, including extent, depth, and shape ~~(Jorgenson et al., 2008).~~(Jorgenson et al., 2008). Abrupt thaw, including both gullies and thermokarst areas, can take different forms and affect the surface methane flux through disturbances in both vegetation and hydrology ~~(Turetsky et al., 2020). Olefeldt et al. (2016) use a definition of thermokarst landscapes, including~~(Turetsky et al., 2020). Olefeldt et al. (2016) describe thermokarst landscapes, which include thermo-erosion gullies characterized by lateral movement of sediments, similar to the gully described in our study. ~~Olefeldt et al. (2016)~~Olefeldt et al. (2016) estimate that ~20 % of land areas in the northern permafrost zone are thermokarst landscapes, meaning they are either currently characterized by soil settlement or erosion or prone to developing into thermokarst landforms in the future. Thermokarst landforms have diverse impacts on a landscape, dependent on their type ~~(Kokelj and Jorgenson, 2013). They could form abruptly and rapidly responding to increasing temperatures (Farquharson et al., 2019; Lewkowicz and Way, 2019). Wickland et al. (2020)~~(Kokelj and Jorgenson, 2013). They could form abruptly and rapidly responding to increasing temperatures (Farquharson et al., 2019; Lewkowicz and Way, 2019). Wickland et al. (2020) found a 42 % increase in growing season methane flux from 1949–2018 in a wet polygonal tundra after an increase in thermokarst erosion of ice -wedges. Thermokarst lakes cover large areas across the Boreal zone and in the Arctic and have been reported to be substantial emitters of methane ~~(Wik et al., 2016; Walter Anthony et al., 2018; Engram et al., 2020). These~~(Wik et al., 2016; Walter Anthony et al., 2018; Engram et al., 2020). The findings from thermokarst lakes contrast the results from this study, where erosion causes draining and loss of organic material. ~~Wik et al. (2016)~~ (Fig. 5). Wik et al. (2016) found a mean flux, combining diffusion and ebullition, of ~3.7 mg m^{-2} h^{-1} from thermokarst lakes in the ice-free season. ~~Walter Anthony et al. (2018)~~Walter Anthony et al. (2018) found an accelerating increase in methane fluxes from thermokarst lakes in their modeling of methane in the 21st for the circumpolar region, which ~~also contrasts~~shows that the impacts ~~from~~ on methane in the ~~gully found in Zackenberg Valley~~event of erosion are diverse. It should be

noted that there is a difference in the 'receiving end' of the gully formation between our study and these thermokarst lake studies as the drainage in the Zackenberg valley goes ~~straight out in~~into the ~~major~~ river systems with few or no stagnant ~~reservoir~~reservoirs between.

~~In our calculation of landscape methane fluxes to changes in surface cover, eroded areas stay unvegetated for the remainder of the century. Still, eroded areas may partly be revegetated after stabilizing, which could change the size of the relative sink shown in Fig. 6. Further, methane oxidation could increase the sink in upland areas during the 21st century (Jørgensen et al., 2015; Oh et al., 2020), which could offset some of the increase in mean flux in Zackenberg Valley.~~

5 Conclusions

In this study, we have summarized 14 measurement-years of methane fluxes and several short-term campaigns, which provide a unique insight into the large variability in methane fluxes in a high Arctic tundra landscape of Zackenberg Valley. We have combined July–August measurements from a monitoring site running from 2006–2019 with detailed ~~single-year~~ measurements of the most common vegetation types in the valley to estimate valley-wide methane fluxes over the period. For the valley, the net emission of methane in July–August shows differences by nearly a factor of ~~10~~4 between individual years (2006–2019). Consistently dry or wet surfaces may remain relatively stable in terms of methane fluxes over the period, as indicated by the data from previous site-specific campaigns in the valley. However, the large areas covering the boundary between these ~~host~~hosts highly variable methane fluxes, significantly impacting methane fluxes ~~at the~~on a landscape ~~-~~scale. Future ~~multiyear~~multi-year campaigns should focus on measuring the full gradient from wet fens to dry heath to improve estimations of landscape methane fluxes, as the fluxes from different surface classes may respond differently to changes in environmental conditions, such as moisture, temperature, snow cover.

Observations from recently eroded gully revealed a small source of methane in this type of landscape. Rapid export of carbon-rich soils and an effective drainage system in the gully are likely the main reasons for the limited methane fluxes.

With rising temperatures in Zackenberg Valley, methane emissions are expected to increase drastically during the 21st century. The warming increases permafrost thaw, which could increase surface erosion in the valley. When compared, our findings show the increase in methane emission from undisturbed fen areas has a much larger impact on the valley-wide fluxes than surface erosion~~, even if riverbanks are heavily eroded.~~. Increased erosion could offset some of the rise in methane fluxes from the valley, but this would require large-scale impacts on vegetated surfaces.

This study shows the importance of ~~multiyear~~multi-year methane monitoring with wide spatial coverage, as interannual variability is substantial when considering a full composite landscape even in a single valley in the Arctic.

Data and code availability

Data from the GEM ClimateBasis and GeoBasis Zackenberg subprograms used in this manuscript are free and open data, available at https://data.g-e-m.dk/ (registration needed). The data are licensed with terms of use under the Creative Commons CC-BY-SA license. Processed data and scripts used for the analyses are available ~~at https://github.com/schellers/Multidecadal-growing-season-fluxes-of-a-high-Arctic-tundra/raw/main/Data_and_code_Multidecadal_growing_season_fluxes_of_a_high_Arctic_tundra.zip.~~

from the corresponding author upon reasonable request. Direct links to the GEM data sources are listed here:

AC Water level automatic: https://doi.org/10.17897/mj7b-z461

AC Water level manual: https://doi.org/10.17897/6hcp-m521

Air temperature, 200cm – 60min average: https://doi.org/10.17897/xv96-hc57

Flux monitoring – AC: https://doi.org/10.17897/430p-ds31

Mix-1 Soil moisture: https://doi.org/10.17897/ennb-t831

Snow cover (Central area): https://doi.org/10.17897/499c-h459

Soil temperature, 20cm – 60min average: https://doi.org/10.17897/xw7c-na36

Author contribution

JHS, MM, and TRC designed the study, and JHS performed the analyses and created figures and tables. HHC helped ~~to interpret~~interpreting the geomorphological processes. JHS wrote the manuscript with contributions from all co-authors.

Competing interests

The authors declare that they have no conflict of interest.

Acknowledgments

This study was supported by the Faculty of Science and Technology and the thematic centers iCLIMATE and ARC at Aarhus University. The authors furthermore acknowledge the use of data from the Greenland Ecosystem Monitoring (GEM) database and are grateful for field support provided by the Zackenberg Research Station.

References

Abermann, J., Hansen, B., Lund, M., Wacker, S., Karami, M., and Cappelen, J.: Hotspots and key periods of Greenland climate change during the past six decades, Ambio, 46, 3-11, doi: 10.1007/s13280-016-0861-y, 2017.

AMAP: Snow, Water and Permafrost in the Arctic (SWIPA) 2017, Oslo, Norway, 269 pp., 2017.

Andresen, C. G., Lara, M. J., Tweedie, C. E., and Lougheed, V. L.: Rising plant-mediated methane emissions from arctic wetlands, Global Change Biology, 23, 1128-1139, doi: 10.1111/gcb.13469, 2017.

Bartlett, K. B., Crill, P. M., Sass, R. L., Harriss, R. C., and Dise, N. B.: Methane emissions from tundra environments in the Yukon-Kuskokwim delta, Alaska, Journal of Geophysical Research, 97, 16645-16660, doi: 10.1029/91jd00610, 1992.

Bay, C.: Vegetation mapping of Zackenberg valley, northeast Greenland, Danish Polar Center and Botanical Museum, University of Copenhagen, 1998.

Bosse, U., and Frenzel, P.: CH4 emissions from a West Siberian mire, Suo, 52, 99-114, 2001.

Cable, S., Christiansen, H. H., Westergaard-Nielsen, A., Kroon, A., and Elberling, B.: Geomorphological and cryostratigraphical analyses of the Zackenberg Valley, NE Greenland and significance of Holocene alluvial fans, Geomorphology, 303, 504-523, doi: 10.1016/j.geomorph.2017.11.003, 2018.

Christensen, T. R.: Methane emission from Arctic tundra, Biogeochemistry, 21, 117-139, doi: 10.1007/bf00000874, 1993.

Christensen, T. R., Friborg, T., Sommerkorn, M., Kaplan, J., Illeris, L., Søgaard, H., Nordstrøm, C., and Jonasson, S.: Trace gas exchange in a high-arctic valley 1. Variations in CO2 and CH4 flux between tundra vegetation types, Global Biogeochemical Cycles, 14, 701-713, doi: 10.1029/1999gb001134, 2000.

Christensen, T. R., Johansson, T. R., Akerman, H. J., Mastepanov, M., Malmer, N., Friborg, T., Crill, P., and Svensson, B. H.: Thawing sub-arctic permafrost: Effects on vegetation and methane emissions, Geophysical Research Letters, 31, doi: 10.1029/2003gl018680, 2004.

Christensen, T. R.: Climate science: Understand Arctic methane variability, Nature, 509, 279-281, doi: 10.1038/509279a, 2014.

Christensen, T. R., Arndal, M. F., and Topp-Jørgensen, E.: Greenland Ecosystem Monitoring Annual Report Cards 2019, DCE – Danish Centre for Environment and Energy, Aarhus University, Aarhus, Denmark, 40 pp, 2020a.

Christensen, T. R., Lund, M., Skov, K., Abermann, J., López-Blanco, E., Scheller, J., Scheel, M., Jackowicz-Korczynski, M., Langley, K., Murphy, M. J., and Mastepanov, M.: Multiple Ecosystem Effects of Extreme Weather Events in the Arctic, Ecosystems, doi: 10.1007/s10021-020-00507-6, 2020b.

Christiansen, H. H., Sigsgaard, C., Humlum, O., Rasch, M., and Hansen, B. U.: Permafrost and Periglacial Geomorphology at Zackenberg, in: High-Arctic Ecosystem Dynamics in a Changing Climate, Advances in Ecological Research, 151-174, 2008.

COWI: eBee saves the day: mapping Greenland's Zackenberg Research Station https://www.sensefly.com/app/uploads/2017/11/eBee_saves_day_mapping_greenlands_zackenberg_research_station.pdf, 2015.

Crill, P. M., Bartlett, K. B., Harriss, R. C., Gorham, E., Verry, E. S., Sebacher, D. I., Madzar, L., and Sanner, W.: Methane flux from Minnesota peatlands, Global Biogeochemical Cycles, 2, 371-384, doi: 10.1029/gb002i004p00371, 1988.

Docherty, C. L., Hannah, D. M., Riis, T., Leth, S. R., and Milner, A. M.: Large thermo-erosional tunnel for a river in northeast Greenland, Polar Science, 14, 83-87, doi: 10.1016/j.polar.2017.08.001, 2017.

Ehhalt, D. H.: The atmospheric cycle of methane, Tellus, 26, 58-70, doi: 10.3402/tellusa.v26i1-2.9737, 1974.

Elberling, B., Tamstorf, M. P., Michelsen, A., Arndal, M. F., Sigsgaard, C., Illeris, L., Bay, C., Hansen, B. U., Christensen, T. R., Hansen, E. S., Jakobsen, B. H., and Beyens, L.: Soil and Plant Community-Characteristics and Dynamics at Zackenberg, in: Advances in Ecological Research: High-Arctic Ecosystem Dynamics in a Changing Climate, Elsevier, 223-248, 2008.

Engram, M., Anthony, K. M. W., Sachs, T., Kohnert, K., Serafimovich, A., Grosse, G., and Meyer, F. J.: Remote sensing northern lake methane ebullition, Nature Climate Change, doi: 10.1038/s41558-020-0762-8, 2020.

Falk, J. M., Schmidt, N. M., and Ström, L.: Effects of simulated increased grazing on carbon allocation patterns in a high arctic mire, Biogeochemistry, 119, 229-244, doi: 10.1007/s10533-014-9962-5, 2014.

Falk, J. M., Schmidt, N. M., Christensen, T. R., and Ström, L.: Large herbivore grazing affects the vegetation structure and greenhouse gas balance in a high arctic mire, Environ Res Lett, 10, doi: 10.1088/1748-9326/10/4/045001, 2015.

Fan, S. M., Wofsy, S. C., Bakwin, P. S., Jacob, D. J., Anderson, S. M., Kebabian, P. L., McManus, J. B., Kolb, C. E., and Fitzjarrald, D. R.: Micrometeorological measurements of CH4 and CO2 exchange between the atmosphere and subarctic tundra, Journal of Geophysical Research, 97, 16627-16643, doi: 10.1029/91jd02531, 1992.

Farquharson, L. M., Romanovsky, V. E., Cable, W. L., Walker, D. A., Kokelj, S. V., and Nicolsky, D.: Climate Change Drives Widespread and Rapid Thermokarst Development in Very Cold Permafrost in the Canadian High Arctic, Geophysical Research Letters, 46, 6681-6689, doi: 10.1029/2019gl082187, 2019.

Friborg, T., Christensen, T. R., Hansen, B. U., Nordstrøm, C., and Søgaard, H.: Trace gas exchange in a high-Arctic valley 2. Landscape CH4 fluxes measured and modeled using eddy correlation data, Global Biogeochemical Cycles, 14, 715-723, doi: 10.1029/1999gb001136, 2000.

Geng, M. S., Christensen, J. H., and Christensen, T. R.: Potential future methane emission hot spots in Greenland, Environ Res Lett, 14, 035001, doi: 10.1088/1748-9326/aaf34b, 2019.

Grøndahl, L., Friborg, T., Christensen, T. R., Ekberg, A., Elberling, B., Illeris, L., Nordstrøm, C., Rennermalm, Å., Sigsgaard, C., and Søgaard, H.: Spatial and inter-annual variability of trace gas fluxes in a heterogeneous high-arctic landscape, in: Advances in Ecological Research: High-Arctic Ecosystem Dynamics in a Changing Climate, Elsevier, 473-498, 2008.

Hansen, B. U., Sigsgaard, C., Rasmussen, L., Cappelen, J., Hinkler, J., Mernild, S. H., Petersen, D., Tamstorf, M. P., Rasch, M., and Hasholt, B.: Present-Day Climate at Zackenberg, in: Advances in Ecological Research: High-Arctic Ecosystem Dynamics in a Changing Climate, Elsevier, 111-149, 2008.

Hartley, I. P., Hill, T. C., Wade, T. J., Clement, R. J., Moncrieff, J. B., Prieto-Blanco, A., Disney, M. I., Huntley, B., Williams, M., Howden, N. J. K., Wookey, P. A., and Baxter, R.: Quantifying landscape-level methane fluxes in subarctic Finland using a multiscale approach, Global Change Biology, 21, 3712-3725, doi: 10.1111/gcb.12975, 2015.

Heikkinen, J. E. P., Virtanen, T., Huttunen, J. T., Elsakov, V., and Martikainen, P. J.: Carbon balance in East European tundra, Global Biogeochemical Cycles, 18, doi: 10.1029/2003gb002054, 2004.

IPCC: Climate Change The IPCC Scientific Assessment, Intergovernmental Panel on Climate Change, Cambridge, 1990.

Jackowicz-Korczynski, M., Christensen, T. R., Bäckstrand, K., Crill, P., Friborg, T., Mastepanov, M., and Ström, L.: Annual cycle of methane emission from a subarctic peatland, Journal of Geophysical Research, 115, G02009, doi: 10.1029/2008jg000913, 2010.

Joabsson, A., and Christensen, T. R.: Methane emissions from wetlands and their relationship with vascular plants: an Arctic example, Global Change Biology, 7, 919-932, doi: 10.1046/j.1354-1013.2001.00044.x, 2001.

Jorgenson, M. T., Schur, Y. L., and Osterkamp, T. E.: Thermokarst in Alaska, Ninth International Conference on Permafrost, Fairbanks, 2008, 869-876,

Jørgensen, C. J., Lund Johansen, K. M., Westergaard-Nielsen, A., and Elberling, B.: Net regional methane sink in High Arctic soils of northeast Greenland, Nature Geoscience, 8, 20-23, doi: 10.1038/ngeo2305, 2015.

Kokelj, S. V., and Jorgenson, M. T.: Advances in Thermokarst Research, Permafrost and Periglacial Processes, 24, 108-119, doi: 10.1002/ppp.1779, 2013.

Lewkowicz, A. G., and Way, R. G.: Extremes of summer climate trigger thousands of thermokarst landslides in a High Arctic environment, Nature Communications, 10, 1329, doi: 10.1038/s41467-019-09314-7, 2019.

Livingston, G., and Hutchinson, G.: Enclosure-based measurement of trace gas exchange: applications and sources of error, in: Biogenic trace gases: measuring emissions from soil and water, edited by: Matson, P. A. a. H., R.C., Blackwell Science Ltd., 14-51, 1995.

Mastepanov, M., Sigsgaard, C., Dlugokencky, E. J., Houweling, S., Ström, L., Tamstorf, M. P., and Christensen, T. R.: Large tundra methane burst during onset of freezing, Nature, 456, 628-630, doi: 10.1038/nature07464, 2008.

Mastepanov, M., Sigsgaard, C., Mastepanov, M., Ström, L., Tamstorf, M. P., Lund, M., and Christensen, T. R.: Revisiting factors controlling methane emissions from high-Arctic tundra, Biogeosciences, 10, 5139-5158, doi: 10.5194/bg-10-5139-2013, 2013.

Mastepanov, M., Pirk, N., Lopez-Blanco, E., Skov, K., Rudd, D., Jackowicz-Korczynski, M., Tamstorf, M., Scheller, J., and Christensen, T. R.: Fifteen years of methane flux measurements in high-arctic tundra, in prep.

Meltofte, H., Christensen, T. R., Elberling, B., Forchhammer, M. C., and Rasch, M.: Introduction, in: Advances in Ecological Research: High-Arctic Ecosystem Dynamics in a Changing Climate, Elsevier, 1-12, 2008.

Meltofte, H., and Rasch, M.: The Study Area at Zackenberg, in: Advances in Ecological Research: High-Arctic Ecosystem Dynamics in a Changing Climate, Elsevier, 101-110, 2008.

Morozumi, T., Shingubara, R., Suzuki, R., Kobayashi, H., Tei, S., Takano, S., Fan, R., Liang, M., Maximov, T., and Sugimoto, A.: Estimating methane emissions using vegetation mapping in the taiga-tundra boundary of a north-eastern Siberian lowland, Tellus B: Chemical and Physical Meteorology, 71, 1581004, doi: 10.1080/16000889.2019.1581004, 2019.

Morrissey, L. A., and Livingston, G. P.: Methane emissions from Alaska Arctic tundra: An assessment of local spatial variability, Journal of Geophysical Research: Atmospheres, 97, 16661-16670, doi: 10.1029/92jd00063, 1992.

Oh, Y., Zhuang, Q. L., Liu, L. C., Welp, L. R., Lau, M. C. Y., Onstott, T. C., Medvigy, D., Bruhwiler, L., Dlugokencky, E. J., Hugelius, G., D'Imperio, L., and Elberling, B.: Reduced net methane emissions due to microbial methane oxidation in a warmer Arctic, Nature Climate Change, 10, 317-321, doi: 10.1038/s41558-020-0734-z, 2020.

Olefeldt, D., Turetsky, M. R., Crill, P. M., and McGuire, A. D.: Environmental and physical controls on northern terrestrial methane emissions across permafrost zones, Global Change Biology, 19, 589-603, doi: 10.1111/gcb.12071, 2013.

Olefeldt, D., Goswami, S., Grosse, G., Hayes, D., Hugelius, G., Kuhry, P., McGuire, A. D., Romanovsky, V. E., Sannel, A. B., Schuur, E. A., and Turetsky, M. R.: Circumpolar distribution and carbon storage of thermokarst landscapes, Nature Communications, 7, 13043, doi: 10.1038/ncomms13043, 2016.

Palmtag, J., Hugelius, G., Lashchinskiy, N., Tamstorf, M. P., Richter, A., Elberling, B., and Kuhry, P.: Storage, landscape distribution, and burial history of soil organic matter in contrasting areas of continuous permafrost, Arctic, Antarctic, and Alpine Research, 47, 71-88, doi: 10.1657/aaar0014-027, 2015.

Parmentier, F., Van Huissteden, J., Van Der Molen, M., Schaepman-Strub, G., Karsanaev, S., Maximov, T., and Dolman, A.: Spatial and temporal dynamics in eddy covariance observations of methane fluxes at a tundra site in northeastern Siberia, Journal of Geophysical Research, 116, doi: 10.1029/2010jg001637, 2011.

Pedersen, S. H., Tamstorf, M. P., Abermann, J., Westergaard-Nielsen, A., Lund, M., Skov, K., Sigsgaard, C., Mylius, M. R., Hansen, B. U., Liston, G. E., and Schmidt, N. M.: Spatiotemporal Characteristics of Seasonal Snow Cover in Northeast Greenland from in Situ Observations, Arctic, Antarctic, and Alpine Research, 48, 653-671, doi: 10.1657/aaar0016-028, 2016.

Pirk, N., Mastepanov, M., Parmentier, F. J. W., Lund, M., Crill, P., and Christensen, T. R.: Calculations of automatic chamber flux measurements of methane and carbon dioxide using short time series of concentrations, Biogeosciences, 13, 903-912, doi: 10.5194/bg-13-903-2016, 2016a.

Pirk, N., Tamstorf, M. P., Lund, M., Mastepanov, M., Pedersen, S. H., Mylius, M. R., Parmentier, F. J. W., Christiansen, H. H., and Christensen, T. R.: Snowpack fluxes of methane and carbon dioxide from high Arctic tundra, Journal of Geophysical Research: Biogeosciences, 121, 2886-2900, doi: 10.1002/2016jg003486, 2016b.

Roulet, N. T., Jano, A., Kelly, C., Klinger, L., Moore, T., Protz, R., Ritter, J., and Rouse, W.: Role of the Hudson Bay lowland as a source of atmospheric methane, Journal of Geophysical Research: Atmospheres, 99, 1439-1454, doi: 10.1029/93jd00261, 1994.

Sachs, T., Wille, C., Boike, J., and Kutzbach, L.: Environmental controls on ecosystem-scale CH4 emission from polygonal tundra in the Lena River Delta, Siberia, Journal of Geophysical Research, 113, doi: 10.1029/2007jg000505, 2008.

Schneider, J., Grosse, G., and Wagner, D.: Land cover classification of tundra environments in the Arctic Lena Delta based on Landsat 7 ETM+ data and its application for upscaling of methane emissions, Remote Sensing of Environment, 113, 380-391, doi: 10.1016/j.rse.2008.10.013, 2009.

Schuur, E. A., McGuire, A. D., Schadel, C., Grosse, G., Harden, J. W., Hayes, D. J., Hugelius, G., Koven, C. D., Kuhry, P., Lawrence, D. M., Natali, S. M., Olefeldt, D., Romanovsky, V. E., Schaefer, K., Turetsky, M. R., Treat, C. C., and Vonk, J. E.: Climate change and the permafrost carbon feedback, Nature, 520, 171-179, doi: 10.1038/nature14338, 2015.

Shakhova, N., Semiletov, I., Leifer, I., Sergienko, V., Salyuk, A., Kosmach, D., Chernykh, D., Stubbs, C., Nicolsky, D., Tumskoy, V., and Gustafsson, Ö.: Ebullition and storm-induced methane release from the East Siberian Arctic Shelf, Nature Geoscience, 7, 64-70, doi: 10.1038/ngeo2007, 2014.

Stiegler, C., Lund, M., Christensen, T. R., Mastepanov, M., and Lindroth, A.: Two years with extreme and little snowfall: effects on energy partitioning and surface energy exchange in a high-Arctic tundra ecosystem, The Cryosphere, 10, 1395-1413, doi: 10.5194/tc-10-1395-2016, 2016.

Ström, L., Ekberg, A., Mastepanov, M., and Christensen, T. R.: The effect of vascular plants on carbon turnover and methane emissions from a tundra wetland, Global Change Biology, 9, 1185-1192, doi: 10.1046/j.1365-2486.2003.00655.x, 2003.

Ström, L., Tagesson, T., Mastepanov, M., and Christensen, T. R.: Presence of Eriophorum scheuchzeri enhances substrate availability and methane emission in an Arctic wetland, Soil Biol Biochem, 45, 61-70, doi: 10.1016/j.soilbio.2011.09.005, 2012.

Ström, L., Falk, J. M., Skov, K., Jackowicz-Korczynski, M., Mastepanov, M., Christensen, T. R., Lund, M., and Schmidt, N. M.: Controls of spatial and temporal variability in CH4 flux in a high arctic fen over three years, Biogeochemistry, 125, 21-35, doi: 10.1007/s10533-015-0109-0, 2015.

Svensson, B. H., and Rosswall, T.: In situ Methane Production from Acid Peat in Plant Communities with Different Moisture Regimes in a Subarctic Mire, Oikos, 43, 341-350, doi: 10.2307/3544151, 1984.

Søgaard, H., Nordstrøm, C., Friborg, T., and Hansen, B. U.: Trace gas exchange in a high-arctic valley 3. Integrating and scaling CO2 fluxes from canopy to landscape using flux data, footprint modeling, and remote sensing, Global Biogeochemical Cycles, 14, 725-744, doi: 10.1029/1999gb001137, 2000.

Søndergaard, J., Tamstorf, M., Elberling, B., Larsen, M. M., Mylius, M. R., Lund, M., Abermann, J., and Rigét, F.: Mercury exports from a High-Arctic river basin in Northeast Greenland (74°N) largely controlled by glacial lake outburst floods, Science of The Total Environment, 514, 83-91, doi: 10.1016/j.scitotenv.2015.01.097, 2015.

Tagesson, T., Molder, M., Mastepanov, M., Sigsgaard, C., Tamstorf, M. P., Lund, M., Falk, J. M., Lindroth, A., Christensen, T. R., and Ström, L.: Land-atmosphere exchange of methane from soil thawing to soil freezing in a high-Arctic wet tundra ecosystem, Global Change Biology, 18, 1928-1940, doi: 10.1111/j.1365-2486.2012.02647.x, 2012.

Tagesson, T., Mastepanov, M., Mölder, M., Tamstorf, M. P., Eklundh, L., Smith, B., Sigsgaard, C., Lund, M., Ekberg, A., Falk, J. M., Friborg, T., Christensen, T. R., and Ström, L.: Modelling of growing season methane fluxes in a high-Arctic wet tundra ecosystem 1997-2010 using in situ and high-resolution satellite data, Tellus B: Chemical and Physical Meteorology, 65, doi: 10.3402/tellusb.v65i0.19722, 2013.

Taylor, M. A., Celis, G., Ledman, J. D., Bracho, R., and Schuur, E. A. G.: Methane Efflux Measured by Eddy Covariance in Alaskan Upland Tundra Undergoing Permafrost Degradation, Journal of Geophysical Research: Biogeosciences, 123, 2695-2710, doi: 10.1029/2018jg004444, 2018.

Thornton, B. F., Prytherch, J., Andersson, K., Brooks, I. M., Salisbury, D., Tjernström, M., and Crill, P. M.: Shipborne eddy-covariance observations of methane fluxes constrain Arctic sea emissions, Science advances, 6, eaay7934, doi: 10.1126/sciadv.aay7934, 2020.

Tomczyk, A. M., and Ewertowski, M. W.: UAV-based remote sensing of immediate changes in geomorphology following a glacial lake outburst flood at the Zackenberg river, northeast Greenland, Journal of Maps, 16, 86-100, doi: 10.1080/17445647.2020.1749146, 2020.

Tomczyk, A. M., Ewertowski, M. W., and Carrivick, J. L.: Geomorphological impacts of a glacier lake outburst flood in the high arctic Zackenberg River, NE Greenland, Journal of Hydrology, 591, 125300, doi: 10.1016/j.jhydrol.2020.125300, 2020.

Turetsky, M. R., Abbott, B. W., Jones, M. C., Anthony, K. W., Olefeldt, D., Schuur, E. A. G., Grosse, G., Kuhry, P., Hugelius, G., Koven, C., Lawrence, D. M., Gibson, C., Sannel, A. B. K., and McGuire, A. D.: Carbon release through abrupt permafrost thaw, Nature Geoscience, 13, 138-145, doi: 10.1038/s41561-019-0526-0, 2020.

Walter Anthony, K., Schneider von Deimling, T., Nitze, I., Frolking, S., Emond, A., Daanen, R., Anthony, P., Lindgren, P., Jones, B., and Grosse, G.: 21st-century modeled permafrost carbon emissions accelerated by abrupt thaw beneath lakes, Nature Communications, 9, 3262, doi: 10.1038/s41467-018-05738-9, 2018.

Westermann, S., Elberling, B., Højlund Pedersen, S., Stendel, M., Hansen, B. U., and Liston, G. E.: Future permafrost conditions along environmental gradients in Zackenberg, Greenland, The Cryosphere, 9, 719-735, doi: 10.5194/tc-9-719-2015, 2015.

Whalen, S. C., and Reeburgh, W. S.: A methane flux time series for tundra environments, Global Biogeochemical Cycles, 2, 399-409, doi: 10.1029/gb002i004p00399, 1988.

Wickland, K. P., Jorgenson, M. T., Koch, J. C., Kanevskiy, M., and Striegl, R. G.: Carbon dioxide and methane flux in a dynamic Arctic tundra landscape: Decadal-scale impacts of ice-wedge degradation and stabilization, Geophysical Research Letters, 47, e2020GL089894, doi: 10.1029/2020gl089894, 2020.

Wik, M., Varner, R. K., Anthony, K. W., MacIntyre, S., and Bastviken, D.: Climate-sensitive northern lakes and ponds are critical components of methane release, Nature Geoscience, 9, 99-106, doi: 10.1038/ngeo2578, 2016.

Wille, C., Kutzbach, L., Sachs, T., Wagner, D., and Pfeiffer, E. M.: Methane emission from Siberian arctic polygonal tundra: eddy covariance measurements and modeling, Global Change Biology, 14, 1395-1408, doi: 10.1111/j.1365-2486.2008.01586.x, 2008.

Abermann, J., Hansen, B., Lund, M., Wacker, S., Karami, M., and Cappelen, J.: Hotspots and key periods of Greenland climate change during the past six decades, Ambio, 46, 3-11, doi: 10.1007/s13280-016-0861-y, 2017.

AMAP: AMAP assessment 2015: Methane as an Arctic climate forcer, Arctic Monitoring and Assessment Programme (AMAP), Oslo, Norway, Oslo, Norway, 152 pp. pp., 2015.

AMAP: Snow, Water and Permafrost in the Arctic (SWIPA) 2017, Oslo, Norway, 269 pp., 2017.

Andresen, C. G., Lara, M. J., Tweedie, C. E., and Lougheed, V. L.: Rising plant-mediated methane emissions from arctic wetlands, Global Change Biology, 23, 1128-1139, doi: 10.1111/gcb.13469, 2017.

Bartlett, K. B., Crill, P. M., Sass, R. L., Harriss, R. C., and Dise, N. B.: Methane emissions from tundra environments in the Yukon-Kuskokwim delta, Alaska, Journal of Geophysical Research, 97, 16645-16660, doi: 10.1029/91jd00610, 1992.

Bay, C.: Vegetation mapping of Zackenberg valley, northeast Greenland, Danish Polar Center and Botanical Museum, University of Copenhagen, 1998.

Bosse, U., and Frenzel, P.: CH4 emissions from a West Siberian mire, Suo, 52, 99-114, 2001.

Cable, S., Christiansen, H. H., Westergaard-Nielsen, A., Kroon, A., and Elberling, B.: Geomorphological and cryostratigraphical analyses of the Zackenberg Valley, NE Greenland and significance of Holocene alluvial fans, Geomorphology, 303, 504-523, doi: 10.1016/j.geomorph.2017.11.003, 2018.

Christensen, T. R.: Methane emission from Arctic tundra, Biogeochemistry, 21, 117-139, doi: 10.1007/bf00000874, 1993.

Christensen, T. R., Friborg, T., Sommerkorn, M., Kaplan, J., Illeris, L., Søgaard, H., Nordstrøm, C., and Jonasson, S.: Trace gas exchange in a high-arctic valley 1. Variations in CO2 and CH4 flux between tundra vegetation types, Global Biogeochemical Cycles, 14, 701-713, doi: 10.1029/1999gb001134, 2000.

Christensen, T. R., Johansson, T. R., Akerman, H. J., Mastepanov, M., Malmer, N., Friborg, T., Crill, P., and Svensson, B. H.: Thawing sub-arctic permafrost: Effects on vegetation and methane emissions, Geophysical Research Letters, 31, doi: 10.1029/2003gl018680, 2004.

Christensen, T. R.: Climate science: Understand Arctic methane variability, Nature, 509, 279-281, doi: 10.1038/509279a, 2014.

Christensen, T. R., Arndal, M. F., and Topp-Jørgensen, E.: Greenland Ecosystem Monitoring Annual Report Cards 2019, DCE – Danish Centre for Environment and Energy, Aarhus University, Aarhus, Denmark, 40 pp, 2020a.

Christensen, T. R., Lund, M., Skov, K., Abermann, J., López-Blanco, E., Scheller, J., Scheel, M., Jackowicz-Korczynski, M., Langley, K., Murphy, M. J., and Mastepanov, M.: Multiple Ecosystem Effects of Extreme Weather Events in the Arctic, Ecosystems, doi: 10.1007/s10021-020-00507-6, 2020b.

Christiansen, H. H., Sigsgaard, C., Humlum, O., Rasch, M., and Hansen, B. U.: Permafrost and Periglacial Geomorphology at Zackenberg, in: High-Arctic Ecosystem Dynamics in a Changing Climate, Advances in Ecological Research, 151-174, 2008.

COWI: eBee saves the day: mapping Greenland's Zackenberg Research Station https://www.sensefly.com/app/uploads/2017/11/eBee_saves_day_mapping_greenlands_zackenberg_research_station.pdf, 2015.

Crill, P. M., Bartlett, K. B., Harriss, R. C., Gorham, E., Verry, E. S., Sebacher, D. I., Madzar, L., and Sanner, W.: Methane flux from Minnesota peatlands, Global Biogeochemical Cycles, 2, 371-384, doi: 10.1029/gb002i004p00371, 1988.

Docherty, C. L., Hannah, D. M., Riis, T., Leth, S. R., and Milner, A. M.: Large thermo-erosional tunnel for a river in northeast Greenland, Polar Science, 14, 83-87, doi: 10.1016/j.polar.2017.08.001, 2017.

Ehhalt, D. H.: The atmospheric cycle of methane, Tellus, 26, 58-70, doi: 10.3402/tellusa.v26i1-2.9737, 1974.

Elberling, B., Tamstorf, M. P., Michelsen, A., Arndal, M. F., Sigsgaard, C., Illeris, L., Bay, C., Hansen, B. U., Christensen, T. R., Hansen, E. S., Jakobsen, B. H., and Beyens, L.: Soil and Plant Community-Characteristics and Dynamics at Zackenberg, in: Advances in Ecological Research: High-Arctic Ecosystem Dynamics in a Changing Climate, Elsevier, 223-248, 2008.

Engram, M., Anthony, K. M. W., Sachs, T., Kohnert, K., Serafimovich, A., Grosse, G., and Meyer, F. J.: Remote sensing northern lake methane ebullition, Nature Climate Change, doi: 10.1038/s41558-020-0762-8, 2020.

Falk, J. M., Schmidt, N. M., and Ström, L.: Effects of simulated increased grazing on carbon allocation patterns in a high arctic mire, Biogeochemistry, 119, 229-244, doi: 10.1007/s10533-014-9962-5, 2014.

Falk, J. M., Schmidt, N. M., Christensen, T. R., and Ström, L.: Large herbivore grazing affects the vegetation structure and greenhouse gas balance in a high arctic mire, Environ Res Lett, 10, doi: 10.1088/1748-9326/10/4/045001, 2015.

Fan, S. M., Wofsy, S. C., Bakwin, P. S., Jacob, D. J., Anderson, S. M., Kebabian, P. L., McManus, J. B., Kolb, C. E., and Fitzjarrald, D. R.: Micrometeorological measurements of CH4 and CO2 exchange between the atmosphere and subarctic tundra, Journal of Geophysical Research, 97, 16627-16643, doi: 10.1029/91jd02531, 1992.

Farquharson, L. M., Romanovsky, V. E., Cable, W. L., Walker, D. A., Kokelj, S. V., and Nicolsky, D.: Climate Change Drives Widespread and Rapid Thermokarst Development in Very Cold Permafrost in the Canadian High Arctic, Geophysical Research Letters, 46, 6681-6689, doi: 10.1029/2019gl082187, 2019.

Friborg, T., Christensen, T. R., Hansen, B. U., Nordstrøm, C., and Søgaard, H.: Trace gas exchange in a high-Arctic valley 2. Landscape CH4 fluxes measured and modeled using eddy correlation data, Global Biogeochemical Cycles, 14, 715-723, doi: 10.1029/1999gb001136, 2000.

Geng, M. S., Christensen, J. H., and Christensen, T. R.: Potential future methane emission hot spots in Greenland, Environ Res Lett, 14, 035001, doi: 10.1088/1748-9326/aaf34b, 2019.

Grøndahl, L., Friborg, T., Christensen, T. R., Ekberg, A., Elberling, B., Illeris, L., Nordstrøm, C., Rennermalm, Å., Sigsgaard, C., and Søgaard, H.: Spatial and inter-annual variability of trace gas fluxes in a heterogeneous high-arctic landscape, in: Advances in Ecological Research: High-Arctic Ecosystem Dynamics in a Changing Climate, Elsevier, 473-498, 2008.

Hartley, I. P., Hill, T. C., Wade, T. J., Clement, R. J., Moncrieff, J. B., Prieto-Blanco, A., Disney, M. I., Huntley, B., Williams, M., Howden, N. J. K., Wookey, P. A., and Baxter, R.: Quantifying landscape-level methane fluxes in subarctic Finland using a multiscale approach, Global Change Biology, 21, 3712-3725, doi: 10.1111/gcb.12975, 2015.

Heikkinen, J. E. P., Virtanen, T., Huttunen, J. T., Elsakov, V., and Martikainen, P. J.: Carbon balance in East European tundra, Global Biogeochemical Cycles, 18, doi: 10.1029/2003gb002054, 2004.

IPCC: Climate Change The IPCC Scientific Assessment, Intergovernmental Panel on Climate Change, Cambridge, 1990.

Jackowicz-Korczynski, M., Christensen, T. R., Bäckstrand, K., Crill, P., Friborg, T., Mastepanov, M., and Ström, L.: Annual cycle of methane emission from a subarctic peatland, Journal of Geophysical Research, 115, G02009, doi: 10.1029/2008jg000913, 2010.

Joabsson, A., and Christensen, T. R.: Methane emissions from wetlands and their relationship with vascular plants: an Arctic example, Global Change Biology, 7, 919-932, doi: 10.1046/j.1354-1013.2001.00044.x, 2001.

Jorgenson, M. T., Schur, Y. L., and Osterkamp, T. E.: Thermokarst in Alaska, Ninth International Conference on Permafrost, Fairbanks, 2008, 869-876,

Jørgensen, C. J., Lund Johansen, K. M., Westergaard-Nielsen, A., and Elberling, B.: Net regional methane sink in High Arctic soils of northeast Greenland, Nature Geoscience, 8, 20-23, doi: 10.1038/ngeo2305, 2015.

Knoblauch, C., Beer, C., Liebner, S., Grigoriev, M. N., and Pfeiffer, E.-M.: Methane production as key to the greenhouse gas budget of thawing permafrost, Nature Climate Change, 8, 309-312, doi: 10.1038/s41558-018-0095-z, 2018.

Kokelj, S. V., and Jorgenson, M. T.: Advances in Thermokarst Research, Permafrost and Periglacial Processes, 24, 108-119, doi: 10.1002/ppp.1779, 2013.

Lewkowicz, A. G., and Way, R. G.: Extremes of summer climate trigger thousands of thermokarst landslides in a High Arctic environment, Nature Communications, 10, 1329, doi: 10.1038/s41467-019-09314-7, 2019.

Linnet, K.: Estimation of the linear relationship between the measurements of two methods with proportional errors, Statistics in Medicine, 9, 1463-1473, doi: 10.1002/sim.4780091210, 1990.

Livingston, G., and Hutchinson, G.: Enclosure-based measurement of trace gas exchange: applications and sources of error, in: Biogenic trace gases: measuring emissions from soil and water, edited by: Matson, P. A. a. H., R.C., Blackwell Science Ltd., 14-51, 1995.

López-Blanco, E., Jackowicz-Korczynski, M. A., Mastepanov, M., Skov, K., Westergaard-Nielsen, A., Williams, M., and Christensen, T.: Multi-year data-model evaluation reveals the importance of nutrient availability over climate in arctic ecosystem C dynamics, Environ Res Lett, 10.1088/1748-9326/ab865b, 2020.

Mastepanov, M., Sigsgaard, C., Dlugokencky, E. J., Houweling, S., Ström, L., Tamstorf, M. P., and Christensen, T. R.: Large tundra methane burst during onset of freezing, Nature, 456, 628-630, doi: 10.1038/nature07464, 2008.

Mastepanov, M., Sigsgaard, C., Mastepanov, M., Ström, L., Tamstorf, M. P., Lund, M., and Christensen, T. R.: Revisiting factors controlling methane emissions from high-Arctic tundra, Biogeosciences, 10, 5139-5158, doi: 10.5194/bg-10-5139-2013, 2013.

Mastepanov, M., Pirk, N., Lopez-Blanco, E., Skov, K., Rudd, D., Jackowicz-Korczynski, M., Tamstorf, M., Scheller, J., and Christensen, T. R.: Fifteen years of methane flux measurements in high-arctic tundra, in prep.

McGuire, A. D., Christensen, T. R., Hayes, D., Heroult, A., Euskirchen, E., Kimball, J. S., Koven, C., Lafleur, P., Miller, P. A., Oechel, W., Peylin, P., Williams, M., and Yi, Y.: An assessment of the carbon balance of Arctic tundra: comparisons among observations, process models, and atmospheric inversions, Biogeosciences, 9, 3185-3204, doi: 10.5194/bg-9-3185-2012, 2012.

Meltofte, H., Christensen, T. R., Elberling, B., Forchhammer, M. C., and Rasch, M.: Introduction, in: Advances in Ecological Research: High-Arctic Ecosystem Dynamics in a Changing Climate, Elsevier, 1-12, 2008.

Meltofte, H., and Rasch, M.: The Study Area at Zackenberg, in: Advances in Ecological Research: High-Arctic Ecosystem Dynamics in a Changing Climate, Elsevier, 101-110, 2008.

Morozumi, T., Shingubara, R., Suzuki, R., Kobayashi, H., Tei, S., Takano, S., Fan, R., Liang, M., Maximov, T., and Sugimoto, A.: Estimating methane emissions using vegetation mapping in the taiga–tundra boundary of a north-eastern Siberian lowland, Tellus B: Chemical and Physical Meteorology, 71, 1581004, doi: 10.1080/16000889.2019.1581004, 2019.

Morrissey, L. A., and Livingston, G. P.: Methane emissions from Alaska Arctic tundra: An assessment of local spatial variability, Journal of Geophysical Research: Atmospheres, 97, 16661-16670, doi: 10.1029/92jd00063, 1992.

Nisbet, E. G., Manning, M. R., Dlugokencky, E. J., Fisher, R. E., Lowry, D., Michel, S. E., Myhre, C. L., Platt, M., Allen, G., Bousquet, P., Brownlow, R., Cain, M., France, J. L., Hermansen, O., Hossaini, R., Jones, A. E., Levin, I., Manning, A. C., Myhre, G., Pyle, J. A., Vaughn, B. H., Warwick, N. J., and White, J. W. C.: Very Strong. Atmospheric Methane Growth in the 4 Years 2014-2017: Implications for the paris Agreement, Global Biogeochemical Cycles, 33, 318-342, 10.1029/2018gb006009, 2019.

Oh, Y., Zhuang, Q. L., Liu, L. C., Welp, L. R., Lau, M. C. Y., Onstott, T. C., Medvigy, D., Bruhwiler, L., Dlugokencky, E. J., Hugelius, G., D'Imperio, L., and Elberling, B.: Reduced net methane emissions due to microbial methane oxidation in a warmer Arctic, Nature Climate Change, 10, 317-321, doi: 10.1038/s41558-020-0734-z, 2020.

Olefeldt, D., Turetsky, M. R., Crill, P. M., and McGuire, A. D.: Environmental and physical controls on northern terrestrial methane emissions across permafrost zones, Global Change Biology, 19, 589-603, doi: 10.1111/gcb.12071, 2013.

Olefeldt, D., Goswami, S., Grosse, G., Hayes, D., Hugelius, G., Kuhry, P., McGuire, A. D., Romanovsky, V. E., Sannel, A. B., Schuur, E. A., and Turetsky, M. R.: Circumpolar distribution and carbon storage of thermokarst landscapes, Nature Communications, 7, 13043, doi: 10.1038/ncomms13043, 2016.

Parmentier, F., Van Huissteden, J., Van Der Molen, M., Schaepman-Strub, G., Karsanaev, S., Maximov, T., and Dolman, A.: Spatial and temporal dynamics in eddy covariance observations of methane fluxes at a tundra site in northeastern Siberia, Journal of Geophysical Research, 116, doi: 10.1029/2010jg001637, 2011.

Pedersen, S. H., Tamstorf, M. P., Abermann, J., Westergaard-Nielsen, A., Lund, M., Skov, K., Sigsgaard, C., Mylius, M. R., Hansen, B. U., Liston, G. E., and Schmidt, N. M.: Spatiotemporal Characteristics of Seasonal Snow Cover in Northeast Greenland from in Situ Observations, Arctic, Antarctic, and Alpine Research, 48, 653-671, doi: 10.1657/aaar0016-028, 2016.

Pirk, N., Mastepanov, M., Parmentier, F. J. W., Lund, M., Crill, P., and Christensen, T. R.: Calculations of automatic chamber flux measurements of methane and carbon dioxide using short time series of concentrations, Biogeosciences, 13, 903-912, doi: 10.5194/bg-13-903-2016, 2016a.

Pirk, N., Tamstorf, M. P., Lund, M., Mastepanov, M., Pedersen, S. H., Mylius, M. R., Parmentier, F. J. W., Christiansen, H. H., and Christensen, T. R.: Snowpack fluxes of methane and carbon dioxide from high Arctic tundra, Journal of Geophysical Research: Biogeosciences, 121, 2886-2900, doi: 10.1002/2016jg003486, 2016b.

Roulet, N. T., Jano, A., Kelly, C., Klinger, L., Moore, T., Protz, R., Ritter, J., and Rouse, W.: Role of the Hudson Bay lowland as a source of atmospheric methane, Journal of Geophysical Research: Atmospheres, 99, 1439-1454, doi: 10.1029/93jd00261, 1994.

Sachs, T., Wille, C., Boike, J., and Kutzbach, L.: Environmental controls on ecosystem-scale CH4 emission from polygonal tundra in the Lena River Delta, Siberia, Journal of Geophysical Research, 113, doi: 10.1029/2007jg000505, 2008.

Schneider, J., Grosse, G., and Wagner, D.: Land cover classification of tundra environments in the Arctic Lena Delta based on Landsat 7 ETM+ data and its application for upscaling of methane emissions, Remote Sensing of Environment, 113, 380-391, doi: 10.1016/j.rse.2008.10.013, 2009.

Schuur, E. A., McGuire, A. D., Schadel, C., Grosse, G., Harden, J. W., Hayes, D. J., Hugelius, G., Koven, C. D., Kuhry, P., Lawrence, D. M., Natali, S. M., Olefeldt, D., Romanovsky, V. E., Schaefer, K., Turetsky, M. R., Treat, C. C., and Vonk, J. E.: Climate change and the permafrost carbon feedback, Nature, 520, 171-179, doi: 10.1038/nature14338, 2015.

Shakhova, N., Semiletov, I., Leifer, I., Sergienko, V., Salyuk, A., Kosmach, D., Chernykh, D., Stubbs, C., Nicolsky, D., Tumskoy, V., and Gustafsson, Ö.: Ebullition and storm-induced methane release from the East Siberian Arctic Shelf, Nature Geoscience, 7, 64-70, doi: 10.1038/ngeo2007, 2014.

Stiegler, C., Lund, M., Christensen, T. R., Mastepanov, M., and Lindroth, A.: Two years with extreme and little snowfall: effects on energy partitioning and surface energy exchange in a high-Arctic tundra ecosystem, The Cryosphere, 10, 1395-1413, doi: 10.5194/tc-10-1395-2016, 2016.

Ström, L., Ekberg, A., Mastepanov, M., and Christensen, T. R.: The effect of vascular plants on carbon turnover and methane emissions from a tundra wetland, Global Change Biology, 9, 1185-1192, doi: 10.1046/j.1365-2486.2003.00655.x, 2003.

Ström, L., Tagesson, T., Mastepanov, M., and Christensen, T. R.: Presence of Eriophorum scheuchzeri enhances substrate availability and methane emission in an Arctic wetland, Soil Biol Biochem, 45, 61-70, doi: 10.1016/j.soilbio.2011.09.005, 2012.

Ström, L., Falk, J. M., Skov, K., Jackowicz-Korczynski, M., Mastepanov, M., Christensen, T. R., Lund, M., and Schmidt, N. M.: Controls of spatial and temporal variability in CH4 flux in a high arctic fen over three years, Biogeochemistry, 125, 21-35, doi: 10.1007/s10533-015-0109-0, 2015.

Svensson, B. H., and Rosswall, T.: In situ Methane Production from Acid Peat in Plant Communities with Different Moisture Regimes in a Subarctic Mire, Oikos, 43, 341-350, doi: 10.2307/3544151, 1984.

Søgaard, H., Nordstrøm, C., Friborg, T., and Hansen, B. U.: Trace gas exchange in a high-arctic valley 3. Integrating and scaling CO2 fluxes from canopy to landscape using flux data, footprint modeling, and remote sensing, Global Biogeochemical Cycles, 14, 725-744, doi: 10.1029/1999gb001137, 2000.

Søndergaard, J., Tamstorf, M., Elberling, B., Larsen, M. M., Mylius, M. R., Lund, M., Abermann, J., and Rigét, F.: Mercury exports from a High-Arctic river basin in Northeast Greenland (74°N) largely controlled by glacial lake outburst floods, Science of The Total Environment, 514, 83-91, doi: 10.1016/j.scitotenv.2015.01.097, 2015.

Tagesson, T., Molder, M., Mastepanov, M., Sigsgaard, C., Tamstorf, M. P., Lund, M., Falk, J. M., Lindroth, A., Christensen, T. R., and Ström, L.: Land-atmosphere exchange of methane from soil thawing to soil freezing in a high-Arctic wet tundra ecosystem, Global Change Biology, 18, 1928-1940, doi: 10.1111/j.1365-2486.2012.02647.x, 2012.

Tagesson, T., Mastepanov, M., Mölder, M., Tamstorf, M. P., Eklundh, L., Smith, B., Sigsgaard, C., Lund, M., Ekberg, A., Falk, J. M., Friborg, T., Christensen, T. R., and Ström, L.: Modelling of growing season methane fluxes in a high-Arctic wet tundra ecosystem 1997-2010 using in situ and high-resolution satellite data, Tellus B: Chemical and Physical Meteorology, 65, doi: 10.3402/tellusb.v65i0.19722, 2013.

Taylor, M. A., Celis, G., Ledman, J. D., Bracho, R., and Schuur, E. A. G.: Methane Efflux Measured by Eddy Covariance in Alaskan Upland Tundra Undergoing Permafrost Degradation, Journal of Geophysical Research: Biogeosciences, 123, 2695-2710, doi: 10.1029/2018jg004444, 2018.

Thornton, B. F., Prytherch, J., Andersson, K., Brooks, I. M., Salisbury, D., Tjernström, M., and Crill, P. M.: Shipborne eddy covariance observations of methane fluxes constrain Arctic sea emissions, Science advances, 6, eaay7934, doi: 10.1126/sciadv.aay7934, 2020.

Tomczyk, A. M., and Ewertowski, M. W.: UAV-based remote sensing of immediate changes in geomorphology following a glacial lake outburst flood at the Zackenberg river, northeast Greenland, Journal of Maps, 16, 86-100, doi: 10.1080/17445647.2020.1749146, 2020.

Tomczyk, A. M., Ewertowski, M. W., and Carrivick, J. L.: Geomorphological impacts of a glacier lake outburst flood in the high arctic Zackenberg River, NE Greenland, Journal of Hydrology, 591, 125300, doi: 10.1016/j.jhydrol.2020.125300, 2020.

Turetsky, M. R., Abbott, B. W., Jones, M. C., Anthony, K. W., Olefeldt, D., Schuur, E. A. G., Grosse, G., Kuhry, P., Hugelius, G., Koven, C., Lawrence, D. M., Gibson, C., Sannel, A. B. K., and McGuire, A. D.: Carbon release through abrupt permafrost thaw, Nature Geoscience, 13, 138-145, doi: 10.1038/s41561-019-0526-0, 2020.

Walter Anthony, K., Schneider von Deimling, T., Nitze, I., Frolking, S., Emond, A., Daanen, R., Anthony, P., Lindgren, P., Jones, B., and Grosse, G.: 21st-century modeled permafrost carbon emissions accelerated by abrupt thaw beneath lakes, Nature Communications, 9, 3262, doi: 10.1038/s41467-018-05738-9, 2018.

Westermann, S., Elberling, B., Højlund Pedersen, S., Stendel, M., Hansen, B. U., and Liston, G. E.: Future permafrost conditions along environmental gradients in Zackenberg, Greenland, The Cryosphere, 9, 719-735, doi: 10.5194/tc-9-719-2015, 2015.

Whalen, S. C., and Reeburgh, W. S.: A methane flux time series for tundra environments, Global Biogeochemical Cycles, 2, 399-409, doi: 10.1029/gb002i004p00399, 1988.

Wickland, K. P., Jorgenson, M. T., Koch, J. C., Kanevskiy, M., and Striegl, R. G.: Carbon dioxide and methane flux in a dynamic Arctic tundra landscape: Decadal-scale impacts of ice-wedge degradation and stabilization, Geophysical Research Letters, 47, e2020GL089894, doi: 10.1029/2020gl089894, 2020.

Wik, M., Varner, R. K., Anthony, K. W., MacIntyre, S., and Bastviken, D.: Climate-sensitive northern lakes and ponds are critical components of methane release, Nature Geoscience, 9, 99-106, doi: 10.1038/ngeo2578, 2016.

Wille, C., Kutzbach, L., Sachs, T., Wagner, D., and Pfeiffer, E. M.: Methane emission from Siberian arctic polygonal tundra: eddy covariance measurements and modeling, Global Change Biology, 14, 1395-1408, doi: 10.1111/j.1365-2486.2008.01586.x, 2008.